Pacemaker activity in a sensory ending with multiple encoding sites: the cat muscle spindle primary ending

R. W. Banks, M. Hulliger*, K. A. Scheepstra*† and E. Otten†

*Department of Biological Sciences, University of Durham, South Road, Durham DH1 3LE, UK, *Department of Clinical Neurosciences, University of Calgary, 3330 Hospital Drive NW, Calgary, Alberta, Canada T2N 4N1 and †Department of Medical Physiology, University of Groningen, Bloemsingel 10, 9712 KZ Groningen, The Netherlands*

1. A combined physiological, histological and computer modelling study was carried out on muscle spindles of the cat tenuissimus muscle to examine whether there was any correlation between the functional interaction of putative encoding sites, operated separately by static and dynamic fusimotor neurones, and the topological structure of the preterminal branches of the primary sensory ending.

2. Spindles, whose Ia responses to stretch and separate and combined static and dynamic fusimotor stimulation were recorded in physiological experiments, were located *in situ*. Subsequently the ramifications of the sensory ending were reconstructed histologically, and the topology of the branch tree was used in computer simulations of Ia responses to examine the effect of the electrotonic separation of encoding sites on the static–dynamic interaction pattern.

3. Interactions between separate static and dynamic inputs, manifest in responses to combined stimulation, were quantified by a coefficient of interaction (C_1) which, by definition, was 1 for strictly linear summation of separate inputs and zero for maximum occlusion between inputs.

4. For the majority of spindles static–dynamic interactions were characterized by pronounced occlusion ($C_1 < 0{\cdot}35$). In these spindles putative encoding sites (the peripheral heminodes of the branches supplying the intrafusal fibres activated by individual fusimotor efferents) were separated by a minimum conduction path of between three and ten myelinated segments (2–9 nodes of Ranvier). In contrast, significant summation (C_1, ~0·7) was found in only one spindle. In this case putative encoding sites were separated by a single node.

5. Occlusion was not due to encoder saturation and it could not be accounted for by any other known physiological mechanisms (intrafusal fatigue or unloading). It is therefore attributed to competitive pacemaker interaction between encoding sites which are largely selectively operated by static and dynamic fusimotor efferents.

6. Model simulations of real preterminal-branch tree structures confirmed that short conduction paths between encoding sites were associated with manifest summation, whereas longer minimum conduction paths favoured pronounced occlusion.

7. In the extreme, occlusion could be so pronounced as to give rise to negative values of C_1 during critical segments of response cycles. This was associated with lower discharge rates during combined static and dynamic stimulation than the higher of the individual stimulation effects. This phenomenon is referred to as hyperocclusion. Computer simulations demonstrated that hyperocclusion could be accounted for by a slow ionic adaptation process, e.g. by a very slowly activating K^+ conductance.

Both physiological and histological studies have independently led to the conclusion that the primary sensory ending of the mammalian muscle spindle possesses at least two sites where encoding of the afferent response may take place. Crowe & Matthews (1964) offered this as a possible explanation for their observation that the dynamic response to a large-amplitude ramp stretch was often unaffected by static fusimotor stimulation. They argued that the response

to the intrafusal contraction induced by the static fusimotor axon was occluded by the dynamic response, when exceeded by it. The phenomenon was later systematically studied by Lennerstrand (1968) and by Hulliger and co-workers (Hulliger, Matthews & Noth, 1977; Emonet-Dénand, Hulliger, Matthews & Petit, 1977*a*; Hulliger & Noth, 1979), who found that the response elicited by combined stimulation of a pair of dynamic and static fusimotor axons was often no greater than that provoked by the more effective of the two axons acting alone (especially during muscle shortening), and that static-induced modulation of the post-stimulus histogram could be abolished during concomitant dynamic action. The occlusion seen in all these cases was interpreted as the result of antidromic invasion and resetting of a momentarily less active encoding site by spikes that were propagating from a more active site, which thus became the pacemaker for the final output of the afferent axon (see Eagles & Purple, 1974).

For this explanation to be correct, it may be noted that there should exist separate static and dynamic effectors and that each should have separate access to the common Ia afferent axon whose terminals form the primary ending. Both of these prerequisites have now been shown to be the normal condition, at least in the tenuissimus muscle of the cat. Banks (1994*a*) reviews the evidence that dynamic axons, whether fusimotor (γ) or skeletofusimotor (β), almost exclusively supply the bag_1 type of intrafusal muscle fibre, whereas static axons only supply the bag_2 and chain types of fibre, either separately or together. Detailed examination of the distribution of preterminal and terminal branches of afferent axons using serial sections and teased, silver-impregnated preparations revealed that the division of the Ia axon into first-order branches was usually dichotomous and that the two branches ultimately provided sensory terminals separately to the bag_1 fibre and to the bag_2 and chain fibres (Banks, Barker & Stacey, 1982; Banks, 1986). In consequence, in most spindles the sensory terminals of the static- and dynamic-innervated intrafusal fibres are separated by an appreciable number of myelinated axon segments. On the assumption that the nodes of Ranvier within the preterminal branches are excitable (and here we include the heminodes where the peripheral branches of the axon become unmyelinated), Banks *et al.* (1982) noted that the observed patterns of preterminal branching could form the structural basis for the separation of static and dynamic pacemakers. Support for the excitability of the nodes was presented by Quick, Kennedy & Poppele (1980), who demonstrated their cytochemical similarity with other sites of known excitability, such as the initial segment of the motoneuron.

Although occlusion is the predominant phenomenon of encoding site interaction in the Ia afferent, Hulliger & Noth (1979) showed that a variable amount of summation also occurs. In an integrated modelling study incorporating electrotonic spread of receptor potentials, Otten, Scheepstra & Hulliger (1995*b*) found that the topology of the preterminal-branching pattern could influence the amount of summation. In particular, electrotonic spread of receptor potentials (actually modelled as currents generated by the receptor terminals) could lead to partial summation, with the magnitude primarily dependent on the length of the axonal path through the preterminal-branch tree. Here we have used the ability to locate individual muscle spindles in the intact tenuissimus muscle of the cat in order to examine whether there is any correlation between the nature of encoding site interactions and the associated preterminal-branch tree structure in real afferent axons. We also compare the observed interactions with computer simulations based on tree structures seen in individual spindles.

Preliminary reports on this study have previously been published (Banks, Hulliger, Otten & Scheepstra, 1993; Banks, Hulliger, Scheepstra & Otten, 1995).

METHODS

Animals and preparation

The experiments were carried out on nine adult cats of both sexes (2·4–5·1 kg weight), anaesthetized throughout with pentobarbitone (40 mg kg^{-1} I.P., supplemented as required I.V.). The tenuissimus muscle of the left hindlimb was prepared according to the mineral oil pool method described by Banks (1991). Up to eleven filaments of L7 and S1 dorsal roots, each containing single-unit afferent axons from spindles in the distal two-thirds of the tenuissimus, were mounted on a 12-way recording electrode. The corresponding ventral roots were split into twenty to thirty filaments, which were individually tested for fusimotor effects in a systematic search of the afferent responses during large-amplitude sinusoidal stretch (2 mm peak to peak, 1 Hz) applied to the distal end of the muscle, while the ventral root filaments were stimulated at a constant rate (100 impulses s^{-1}). Filaments that evoked positive effects were further subdivided if necessary, until functionally single motor axons remained, as judged by all-or-none antidromic spikes and threshold of fusimotor effects. In several instances an all-or-none extrafusal effect was still observed at the same threshold as the fusimotor effect. Such functionally single axons were provisionally identified as skeletofusimotor (β). Confirmation of their nature was usually demonstrable by a residual fusimotor effect after the extrafusal motor unit had been fatigued by a period of stimulation at a high rate.

Muscle afferents were classified as group Ia on the basis of their characteristic response to a muscle twitch and their excitation by dynamic fusimotor neurones, regardless of whether the latter were isolated as functionally single axons or activated in ventral root filaments that also contained skeletomotor fibres. Fusimotor efferents were classified as static or dynamic using the criteria of Emonet-Dénand, Laporte, Matthews & Petit (1977*b*), with the exception that the absence of Ia discharge during muscle shortening and concomitant fusimotor activation could not be relied on as a distinguishing feature of pure dynamic action. This seemed acceptable, since it is a well-known property of the present semi-conservative preparation of the tenuissimus muscle that imposed stretches are poorly transmitted to proximal portions of the muscle. Therefore, in proximal compartments velocities of locally effective stretch and release were almost certainly much lower than in shorter muscles with more uniform mechanical properties.

Control of muscle stretch, fusimotor stimulation and data collection

Experimental parameters of muscle stretch and fusimotor stimulation were controlled by a hybrid signal generator (Frei, Hulliger & Lengacher, 1981), as described by Baumann & Hulliger (1991). Spikes obtained from single afferent axons were filtered, converted to TTL pulses, and the data stored on-line as interspike intervals using an LSI 11/73 computer operating at a sampling rate of 100 kHz. Various patterns of length, motor stimulation and acquisition parameters were used, which were assembled from 8 s cycle periods, the different functions being kept in strict register by a single master clock. Three main classes (T1–T3) of pattern were used: T1, an 8 s triangular conditioning prestretch (7·5 mm peak to peak), followed by an 8 s acquisition period during which a trapezoidal stretch (5 mm peak to peak) was applied; T2 and T3, an 8 s triangular conditioning prestretch, as in T1, followed by a trapezoidal stretch of similar parameters to that of T1 but with the plateau extended by 16 s so as to maintain the muscle at constant length during acquisition from 16 to 24 s. In each case (T1–T3) a gate enabling motor stimulation was open from 2 s before the onset of data acquisition to the end of the data acquisition period (Fig. 1). The conditioning prestretch was chosen to abolish any after-effects resulting from preceding fusimotor stimulation (Baumann, Emonet-Dénand & Hulliger, 1983; Emonet-Dénand, Hunt & Laporte, 1985).

Patterns of motor stimulation

Motor axons that acted on the same primary ending were stimulated in pairs according to defined sequences, during which the stretch and data acquisition cycles were repeated. The axons were either γ or β, and usually there was one dynamic and one static in each pair. For T1 and T3 the sequence of stimulation was: no stimulation (passive response), dynamic alone, static alone, dynamic and static combined, static alone, dynamic alone, dynamic and static combined, no stimulation. The rationale for this particular sequence was to rule out undue systematic influences of order of presentation on the quantitative estimates of discharge rates and of interaction between separate inputs, as for instance, could have arisen from long-lasting adaptation following episodes of high discharge rate (e.g. during stimulation of dynamic efferents).

When the muscle was subjected to trapezoidal stretch during the acquisition period (T1), stimulation rates were constant and typically 100 impulses s^{-1}, both for the dynamic and the static axons. When the muscle was held at constant (extended) length throughout the acquisition period (T3), first the static axon was stimulated at a constant rate (between 25 and 120 impulses s^{-1}) and the dynamic axon at a triangularly modulated rate (mean, 0–80 impulses s^{-1}; modulation, 70–150 impulses s^{-1}) in phase with the acquisition period (Fig. 1, T3). Then the entire cycle was repeated with modulated static (mean, 30–80 impulses s^{-1}; modulation, 30–80 impulses s^{-1}) and constant dynamic (50–150 impulses s^{-1}) stimulation. The actual rates were determined individually for each spindle so as to produce a large amount of overlap in the afferent discharge rates separately elicited by the constant and modulated fusimotor stimulations. Whenever possible, more than one set of stimulation rates was used with each spindle, resulting in different overall discharge rates throughout the acquisition period. The data derived from these are tabulated separately in Table 1*A* where they are referred to comparatively as 'low overall rate' and 'high overall rate'.

For T2 the sequence of stimulation was static alone followed by dynamic alone. In this case the muscle was again held at constant length and the stimulation rate was triangularly modulated. The rate varied from 0 to 150 to 0 impulses s^{-1} in phase with the acquisition period. This protocol was used as a test of afferent

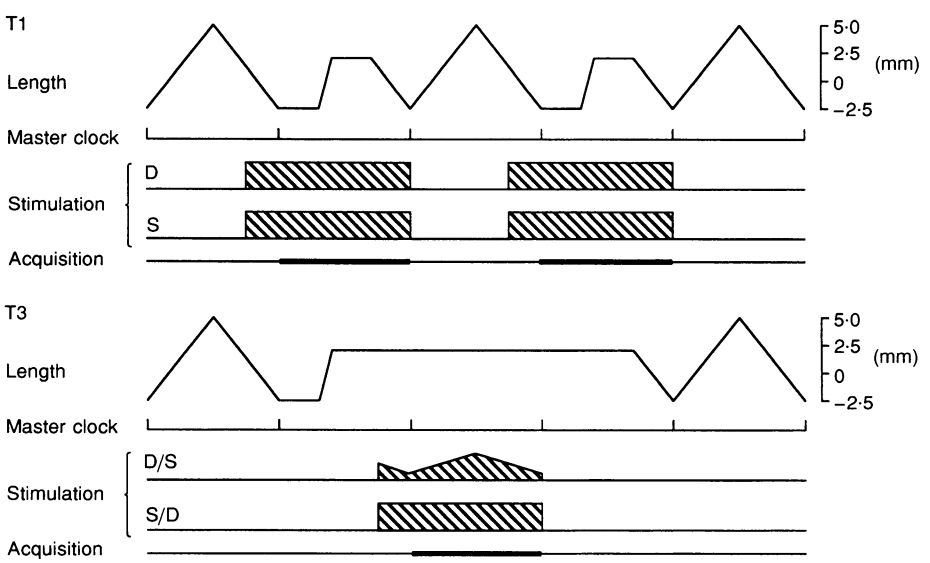

Figure 1. Control of stimulation and data acquisition

Schematic diagram showing protocols for the control of muscle length (calibrated traces), fusimotor stimulation (hatched areas) and data acquisition (thicker bars), whose phase relationships were maintained by reference to a master clock cycle. Note that in T1 the muscle was stretched during data acquisition, whereas in T3 it was held at constant length. D, dynamic stimulation; S, static stimulation. Note also that T3 encompassed two separate stimulation configurations, one with modulated dynamic and constant static stimulation (D/S), the other with modulated static and constant dynamic activation (S/D; see also Figs 4 and 5). T2 (see text) was similar to T3, but only a single channel was used for fusimotor stimulation, triangularly modulated during the acquisition period. See text for full details.

driving by the fusimotor axon, so as to give an indication of which intrafusal fibres were actively contracting, and in particular whether the bag_2 fibre, the chain fibres, or both, were activated by the static axon. A bag_2 fibre, when activated alone, produces biasing of the Ia discharge, which reaches maximum amplitude at stimulation rates of ~50 impulses s^{-1}, the discharge having low variability and showing no sign of phase-locking to ('driving' by) the stimuli. Conversely, chain fibres active alone produce 1 : 1 driving of the Ia discharge, for stimulation rates within a range of ~30 to ~100 impulses s^{-1}, with driving giving way at higher stimulation rates to a very highly variable discharge of mean rate higher than that of the stimulation. Responses that cannot be classified in either of these two categories, for example if only subharmonic driving (1 : 2, 1 : 3, etc.) of Ia discharge rate is present, are attributable to combined activation of bag_2 and chain fibres (see Banks, 1991; Celichowski, Emonet-Dénand, Laporte & Petit, 1994).

Histology

On completion of the series of physiological tests T1–T3 for a particular primary ending, the position of the spindle containing the ending was found by localized stretching and probing the surface of the muscle. The position was marked with an epimysial stitch using fine silk. At the end of the experiment, that part of the muscle containing the located spindles was tied under light tension to a plastic straw, excised and fixed by immersion in Karnovsky's fixative (20% paraformaldehyde, 2·5% glutaraldehyde in 0·1 M sodium phosphate buffer pH 7·3) for about 7 h. Initially the spindles and their nerve supplies were teased out of the surrounding extrafusal fibres before or during secondary fixation in OsO_4. The equatorial region of each spindle, containing the primary ending, could thus be identified, separately embedded in epoxy resin, and serially sectioned longitudinally at 1 μm thickness from a convenient direction. However, some spindles were lost or damaged during teasing, so those derived from the last two experiments were left *in situ*. Approximately 1 cm lengths of muscle centred on the epimysial stitches were then cut out, embedded in resin, and either sectioned transversely and serially throughout or turned to be sectioned longitudinally when the equatorial region of the relevant spindle was approached. After staining with Toluidine Blue, the sections were used to reconstruct the preterminal branching patterns and distributions of the Ia afferents. In most cases the reconstruction was limited to the topological structure of the branching pattern, but for two spindles it was necessary to carry out a more complete reconstruction by superimposing tracings of the sections in order to be certain of the precise distribution of the Ia terminals.

In discussing the possible role of electrotonic coupling of putative encoding sites, we shall subsequently make use of a topological measure of the distance between the sites, which we have called the minimum path length (MPL). This is simply the number of complete nodes of Ranvier in the shortest path connecting the sites. Although the MPL is at present the only available determinant of electrotonic coupling it must be stressed that the coupling would in fact depend on the actual dimensions and cable properties of the internodes that link the encoding sites, but to obtain the necessary data for a detailed electrotonic simulation of actual endings is made difficult by the often contorted nature of the more peripheral branches of the preterminal tree and the labour involved in 3-dimensional reconstruction. However, if we make the simplifying assumption that the specific cable properties are constant throughout the preterminal tree, then the progressive peripheral decrease in internodal diameter and myelin thickness (Quick, Kennedy & Donaldson, 1979) that would result in a decreased electrotonic length would be offset to some extent by the correlated decrease in actual internodal length (Quick *et al.* 1979; Banks *et al.* 1982).

Data analysis

Ia responses were displayed either as profiles of instantaneous discharge rate (as in Figs 3 and 4) or as probability density estimates of discharge rate (see Matthews & Stein, 1969), in either case for a unitary cycle duration of 8 s. Probability density cycle histograms were used exclusively for the calculation of population responses averaged across subsamples or the entire sample of Ia afferents (Figs 2 and 5), as well as for the calculation of coefficient of interaction (C_i) values (see below) and various discharge rate statistics (e.g. Figs 6 and 11). The probability density, rather than the average frequency method, was chosen to avoid the discharge rate-dependent distortions associated with the latter (Matthews & Stein, 1969; Hulliger & Baumann, 1994). Bin widths of probability density histograms were 50 or 200 ms for population response estimates and 200 ms for calculations of C_i and other discharge rate statistics.

In an attempt to relate observed discharge rates to simple measures of sensory preterminal tree topology, multivariate least-squares regression fits were calculated using the downhill simplex method in multidimensions of Nelder & Mead (1965) to compare predicted with experimentally observed discharge rates during combined stimulation (see Fig. 11, and the predicted response profiles in Figs 3*Ag*, 3*Bg*, 4*Ag* and 4*Bg*). Measured discharge rates (R_c, R_h and R_l; see eqn (2)) were calculated as probability density estimates for non-overlapping windows (bins) of 200 ms duration. Discharge rate predictions (eqn (3) in the Discussion) were based on the measured rates (R_h and R_l) during separate static and dynamic stimulation and on an estimate of minimal distance between putative static- and dynamic-operated encoding sites (minimum path length, MPL; see Results).

Measurement of pacemaker interaction

The amount of interaction, either competitive or summative, that occurred between separate inputs (operating putative separate pacemakers) was expressed as a coefficient of interaction (C_i), which was calculated on a bin-by-bin basis using data collected in 200 ms bins:

$$\begin{aligned} C_i &= (R_c - R_s)/R_d \qquad R_s \geqslant R_d \\ C_i &= (R_c - R_d)/R_s \qquad R_d > R_s, \end{aligned} \tag{1}$$

where R_d and R_s are the afferent discharge rates in response to dynamic and static stimulation, respectively, and R_c is the rate in response to combined stimulation. For the following considerations the above expression can be rewritten in the simpler form of:

$$C_i = (R_c - R_h)/R_l, \tag{2}$$

where R_h and R_l are the momentarily higher and lower rates of discharge under separate fusimotor activation, irrespective of type.

The present coefficient of interaction, although derived independently, is formally identical to the coefficient of summation introduced by Gregory, Morgan & Proske (1985) in their study of the tendon organ. In general, one would expect C_i to take values between zero ($R_c = R_h$, pure competition or complete occlusion) and 1 ($R_c = R_h + R_l$, pure summation). However, interpretation of C_i requires some caution. First, it should be emphasized that R_c, R_h and R_l are necessarily obtained separately. Therefore, even if in successive stimulation trials the static and dynamic stimuli have the same intrafusal effects (whether acting singly or together), minor variations in the rates can produce large variations in C_i or

unrealistic values of it (e.g. $C_i > 1$), particularly when R_l is close to zero. For instance, for a discharge rate of 10 impulses s^{-1} the present analysis window of 200 ms would on average encompass only two action potentials, yet normal discharge variability may easily add or take away one event, causing a 50% increase or 100% decrease in discharge rate estimates. To avoid some of these vagaries, computation of C_i values was restricted to discharge rates of $R_l > 20$ impulses s^{-1} (except for Fig. 3*Cf*; see below). Secondly, in principle C_i could obtain negative values, but only if $R_e < R_h$. This might occur again because of minor variations of the type just described, but if well developed, as we shall see was sometimes the case, negative values of C_i would require some other explanation.

Minor variations of a random nature are easily dealt with by averaging, but for C_i to be a useful comparative measure it is necessary either that it is a true constant property of a particular ending, or if it is not, that it can be assigned a characteristic value under comparable conditions. One potentially significant cause of variation in C_i is probabilistic mixing of impulse trains generated independently at separate encoding sites (Eagles & Purple, 1974). Eagles & Purple described the discharge properties of separate encoding sites by probability density functions, with Gaussian, Γ, or Poisson distributions. They found that for Gaussian and Γ functions, when encoding sites supplied a common afferent and were mutually reset by antidromic invasion, the common output was normally determined by the encoder with the intrinsically higher mean rate, but that when there was considerable overlap in the individual probability density functions the mean rate of the common output was slightly increased. Behaviour consistent with this prediction was subsequently found both in spindles (Hulliger & Noth, 1979) and tendon organs (Fukami, 1980). The consequence for C_i is that it would be expected to attain a maximum value when $R_h = R_l$.

It was indeed found that C_i was not an invariant property of a given ending, changing in a systematic phase-dependent manner during response cycles and apparently depending on the difference between separate static- and dynamic-induced discharge rates (see Results). However, since these variations were at least to some extent systematic (and present in all observations; cf. Fig. 6), it seemed justified to calculate approximate average values of C_i to characterize individual response cycles and Ia efferent combinations. To avoid undue influence of low values of R_l (see above), calculation of mean C_i was restricted to segments of the response cycle where the difference in discharge rates ($R_h - R_l$) was < 10 impulses s^{-1}.

Simulations

A model based on likely mechanical properties of intrafusal muscle fibres was used to generate a receptor current associated with each type of fibre. The model was an extension of that developed by Schaafsma, Otten & Van Willigen (1991), modified to include chain fibres in addition to bag_1 and bag_2 types (Scheepstra, Otten, Hulliger & Banks, 1995). The receptor currents in turn generated action potentials in an ionic model based on Frankenhaeuser–Huxley kinetics, modified by the addition of a slow, voltage-dependent K^+ channel with a time constant of 70 ms, to simulate realistic discharge rates (Otten, Hulliger & Scheepstra, 1995*a*). Action potentials were generated at the heminodes of individual afferent trees and propagated through the nodes at realistic speed. The discharge rate of a heminodal pacemaker might be influenced by the receptor current of its own terminal, by that of other terminals spreading passively through the preterminal branches and by antidromic invasion and resetting by central nodal spikes. In addition, impulse traffic was influenced by spike collision and cancellation, when orthodromic and antidromic action potentials occurred simultaneously in a given myelinated segment. The receptor current was assumed not to be reset by antidromic impulse invasion and was therefore modelled as an external current input to the heminodes.

In addition, a very slow hyperpolarizing conductance was included to enable the model to reproduce slow adaptation processes with time constants of around 3 s. This was motivated by recent observations on adaptation of Ia discharge (in the presence or absence of fusimotor biasing) following periods of high-rate antidromic activation of the Ia axon which, demonstrably, caused resetting of static- and dynamic-operated encoding sites (K. A. Scheepstra, M. Hulliger, S. Day & E. Otten, unpublished observations). Formally this hyperpolarizing conductance was modelled as a very slowly activating, voltage-dependent K^+ conductance with the same activation voltage characteristics as the slow K^+ conductance of Otten *et al.* (1995*a*), but with rate coefficients (a and b) of 5×10^{-6}, a factor of 100 less than the corresponding rate constants (a_q and b_q) of the slow (70 ms) conductance. It bears emphasis that this particular implementation is by no means a unique solution of the problem. Formal simulations of other hyperpolarizing processes, such as slow Na^+ inactivation or of an electrogenic Na^+–K^+ pump, would have resulted in comparable model behaviour. For the purposes of the present study the precise mechanism underlying slow adaptation was irrelevant, as long as it was capable of reproducing an adaptation in discharge rate, induced by preceding high-rate impulse activity, since it emerged that certain experimental observations (see below) could indeed be best accounted for on the basis of activity-induced membrane hyperpolarization.

RESULTS

Data were collected from twenty-one Ia afferents, each excited by a static and a dynamic fusimotor efferent. In five cases reliable histology could not be obtained as the spindles were damaged either during dissection or teasing, so that observations on Ia preterminal-branch tree structure could only be made on sixteen spindles. The analysis comparing physiological and histological features is therefore restricted to those sixteen afferents (e.g. Figs 7, 9 and 12), while Ia responses from the remaining five spindles were also used for the analysis of purely physiological properties. Spindles and Ia afferents with established histology were ranked and numbered according to the MPL between putative encoding sites (see below) and are referred to as Ia.1–Ia.16 (see Figs 7 and 9, and cf. Table 1).

Population responses to trapezoidal stretch

To emphasize the generality of the observations to be detailed below, Fig. 2 shows the averaged (population) responses of all the afferents to trapezoidal stretch during maintained stimulation of fusimotor efferents, illustrating the actions of separate (Fig. 2*A b*, *c*, *B b* and *c*) or combined (Fig. 2*A d* and *B d*) activation of static and dynamic efferents. Before considering the main features of static– dynamic interaction effects, the issue of reproducibility of observations has to be addressed, since any systematic effect of order of presentation of stimuli (see Methods) on measured discharge rates during single-fibre or combined fusimotor stimulation could obviously distort any measure of interaction.

Responses of individual primary afferents to repeated, similar combinations of stimulus parameters were highly reproducible; moreover, the order of presentation of the separate static and dynamic stimuli made no apparent difference to the type and magnitude of interaction, as measured by the coefficient of interaction, C_i. This is evident by comparing the two columns of Fig. 2. First (Fig. 2*A*) and second (Fig. 2*B*) presentations of static, dynamic and combined inputs resulted in the averaged responses shown in corresponding pairs (Fig. 2*A a–d* and *B a–d*). The similarity between the members of each pair is apparent, and is confirmed by computing the difference between

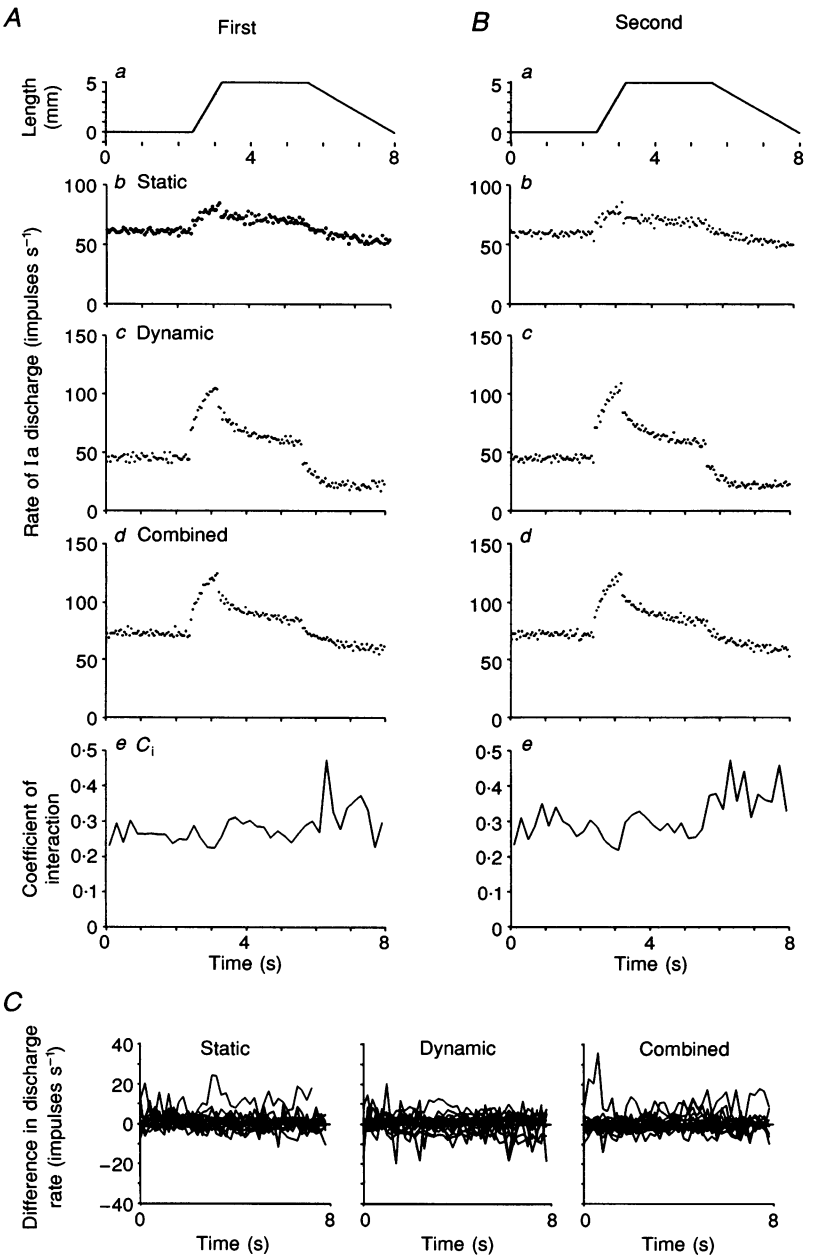

Figure 2. Ia population responses during stretch

Population responses of all ($n = 21$) Ia afferents during the first (*A*) and second data acquisition periods (*B*) of protocol T1 (cf. Methods). *a*, muscle length; *b–d*, responses, averaged using 50 ms bins, during static (*b*), dynamic (*c*), and combined static and dynamic (*d*) fusimotor stimulation; *e*, the coefficient of interaction, C_i, computed from *b–d* (see text) using 200 ms bins; *C*, superimposed plots (200 ms bins) of the difference between the responses from the first and second acquisition periods of individual Ia afferents during static (left), dynamic (middle), and combined (right) fusimotor stimulation showing the reproducibility of consecutive responses. Average discharge rates were estimated using the probability density method (see Methods).

Table 1*A*. Values of the coefficient of interaction (C_i) for each spindle under various stimulus conditions

Afferent no.	MPL	C_i				
		Trapezoidal stretch	Constant length			
			Dynamic modulated/static constant		Static modulated/dynamic constant	
			Low overall rate	High overall rate	Low overall rate	High overall rate
		A	B	C	D	E
Ia.1	**1**	**0·69**	—	**0·42**	0·48	**0·62**
Ia.2	2	0·27	—	—	0·17	0·21
Ia.3	3	0·40	—	—	0·05	0·20
Ia.4	3	0·38	—	0·25	—	0·24
Ia.5	4	0·20	—	—	0·17	0·13
Ia.6	5	0·19	—	—	0·10	0·23
Ia.7	5	0·23	—	—	—	—
Ia.8	5	0·33	0·30	0·27	0·40	—
Ia.9	**6**	**0·35**	0·14	**0·26** *	0·19	**0·42**
	—	—	—	0·26 *	—	—
Ia.10	6	0·25	0·10	—	0·07	0·10 *
	—	—	—	—	—	0·15 *
Ia.11	6	0·24	0·19	0·18	0·17	—
Ia.12	**7**	**0·22** †	—	**0·25**	—	**0·17**
	—	0·27 †	—	—	—	—
Ia.13	**8**	**0·17**	—	**0·11**	—	**0·17**
Ia.14	**9**	**0·21**	—	**0·22**	—	**0·23**
Ia.15	**9**	**0·21** †	—	**0·18** ‡	—	**0·18** ‡
	—	**0·18** †	—	**0·23** ‡	—	**0·15** ‡
Ia.16	9	0·26	—	—	—	—

The use of different rates of stimulation for some spindles at constant length resulted in discharge rates that were relatively low (low overall rate) or high (high overall rate) throughout the acquisition period. * same fusimotor combination stimulated at different rates. † different fusimotor combinations stimulated at the same rate. ‡ different fusimotor combinations stimulated at different rates. Data in bold were used for pairwise comparisons in Table 1*B*.

Table 1*B*. Correlation coefficients (r) for pairwise comparisons of C_i for individual spindles under various comparable conditions

Columns	r	t	d.f.	P
A *vs.* C	0·90	4·938	6	< 0·005
A *vs.* E	0·94	6·397	6	< 0·001
C *vs.* E	0·84	3·796	6	< 0·010

Data shown in bold in Table 1*A*. d.f., degrees of freedom.

Table 1*C*. Spearman's rank correlation coefficient (R_s) for MPL against C_i, corrected for tied values

	R_s	t	d.f.	P
MPL *vs.* A	−0·5727	−2·794	16	< 0·05
MPL *vs.* C	−0·7303	−3·207	9	< 0·05
MPL *vs.* D	−0·1818	−0·489	7	n.s.
MPL *vs.* E	−0·3742	−1·398	12	n.s.

Data from the relevant columns in Table 1*A*.

corresponding first and second responses for individual afferents. The superimposed plots are all centred around differences of 0 impulses s^{-1} (Fig. 2*C*).

The value of C_i, calculated from the population responses, ranged between about 0·25 and 0·5, indicating that in general the interaction between static and dynamic fusimotor effects was dominated by occlusion (see Methods). C_i can be seen to vary according to the phase of the stretch such that there was a slight fall during muscle lengthening when the average dynamic response greatly exceeded the static response. Conversely, during the phase of muscle shortening, when the dynamic response was exceeded by the static response, C_i increased slightly.

Individual responses, and the variability and variation of C_i

Despite the dependence of C_i on the phase of the stretch cycle, the overall responses of individual endings during a trapezoidal stretch showed various degrees of presumed

encoding site interaction ranging from virtually complete occlusion to considerable summation. Examples of these extreme types are shown in Fig. 3, where we also introduce a graphic convention, the interaction band (Fig. 3*A e* and *Be*), which we will subsequently use in comparing the physiological and histological observations. The interaction band (shown by the filled band) is the difference between the response to combined stimulation and the momentarily greater response to either static or dynamic stimulation alone. Comparison with the linear sum of the separate responses (continuous line above the interaction bands in Fig. 3*A e* and *Be*) provides an immediate visual impression of the degree of summation present: hence, the wider the interaction band compared with the open band (between the response to combined stimulation and the summed individual responses), the greater the extent of summation.

The responses shown in Fig. 3 are derived from the primary endings of two spindles that were closely adjacent in the same muscle (Ia.1 and Ia.13 in Figs 7 and 9). In Fig. 3*A* a very high level of summation (shown by a wide interaction band) is exhibited prior to, and throughout, the trapezoidal stretch (Fig. 3*A e* and *f*) by an ending that was driven 1 : 1 by static stimulation at 60 impulses s^{-1} (Fig. 3*A b*). That this extreme degree of summation was intrinsically associated with the primary ending, and was not an artifact arising as a consequence of the driving, is shown by its persistence during higher rate (110 impulses s^{-1}) static stimulation when driving was absent (Fig. 3*B*), and by the fact that the other primary ending (Ia.13), which shows a very high degree of occlusion (Fig. 3*C e* and *f*), was also driven (1 : 2) by static stimulation at 100 impulses s^{-1} (Fig. 3*C b*). The graph of C_i obtained for this latter example of pronounced occlusion (Fig. 3*Cf*; Ia.13) clearly illustrates the need to treat cautiously estimates of C_i calculated for small values of R_i (see Methods). In this case there could be no doubt that with combined fusimotor stimulation the response during shortening was entirely dominated by the static action (cf. Fig. 3*Cd* with *b*). However, when also calculated for R_i values below 20 impulses s^{-1} (see Methods), C_i apparently increased quite dramatically (dashed line in Fig. 3*Cf*). This was readily attributable to the inaccuracy of the measure when both numerator ($R_c - R_h$) and denominator (R_i) are small and easily distorted by inherent measurement inaccuracy.

Finally, it may be noted that driving, though apparently a powerful effect during static stimulation alone (Fig. 3*A b*), was abolished in the combined response of the first ending (Ia.1) by the added input due to dynamic stimulation (Fig. 3*A d*), even when the dynamic response alone was lower than the driven discharge rate (cf. Fig. 3*A c* with *b*). This on its own suggests that in the case of Ia.1 the interaction between static and dynamic inputs featured appreciable summation (cf. Fig. 3*A f* and *Bf*).

The variability of C_i in individual response cycles illustrated in the examples of Fig. 3 was representative of the present sample of Ia afferents. In addition to individual variability between Ia afferents there was a systematic component which is adequately reflected by the estimates of C_i derived from population responses (Figs 2*A e* and *Be*, and 5*A d* and *Bd*). It is worth noting that, in contrast to the observations at constant length (see below), negative values of C_i were virtually never seen in the responses to trapezoidal stretch. As described in Methods, individual combinations of a Ia afferent and a static and dynamic efferent were characterized by an average C_i value. These are listed in Table 1*A* and illustrated in Fig. 12. The main finding was that in the majority of cases occlusion prevailed ($C_i \leqslant 0{\cdot}35$ for 13/16 combinations in Table 1). This finding is further dealt with below, when considering the possible relationship between interaction pattern and preterminal-branch topology.

The size of the coefficient of interaction (C_i) also varied during triangularly modulated stimulation given to one of the fusimotor inputs, while the muscle was held at constant length and the other fusimotor input was stimulated at a constant rate (protocol T3, see Methods). This was so irrespective of whether the static (Fig. 4*A* and *B*) or dynamic (Fig. 4*C*) input was modulated. Again, individual endings exhibited characteristic degrees of summation, generally consistent with those of the same endings responding to trapezoidal stretch. Thus, for example, the ending whose responses are shown in Fig. 4*B* (Ia.1) had the greatest average C_i for this protocol, and is the same ending as that which exhibited extremely high summation during trapezoidal stretch (Fig. 3*A* and *B*; Ia.1). Two features of C_i modulation that were of very common occurrence are also shown by these three sets of responses. First is the tendency for C_i to reach maximum values when the discharge rates evoked by the separate static or dynamic inputs were similar (Fig. 4*A e* and *Be*; see also Fig. 6). Second is the occurrence of the unexpected, indeed surprising, phenomenon that we have called hyperocclusion. In this case, the combined response rate appeared to be dominated by the modulated input to the extent that at very low modulated stimulus rates the combined response rate fell below the level that was evoked by the maintained input acting alone (Fig. 4*B*; see also Fig. 5, and below). It is manifested as negative values of C_i (Fig. 4*Bf*). It bears emphasis that the phenomenon of hyperocclusion was only encountered consistently in responses to tonic combined with modulated fusimotor stimulation at constant length (cf. Fig. 6*B* and *C* with *A*; see also Discussion). Hyperocclusion occurred irrespective of whether the dynamic (Figs 5*B* and 6*B*) or static (Figs 5*A* and 6*C*) input was modulated, but only if the modulated response fell below the maintained response when each was stimulated separately during the corresponding phase of the stimulus protocol.

Hyperocclusion was observed in about half of the combinations of a Ia afferent with a static and a dynamic efferent. Furthermore, the magnitude of the phenomenon was somewhat exaggerated by the measure of interaction, C_i, that was used to quantify it (see Methods). Nevertheless,

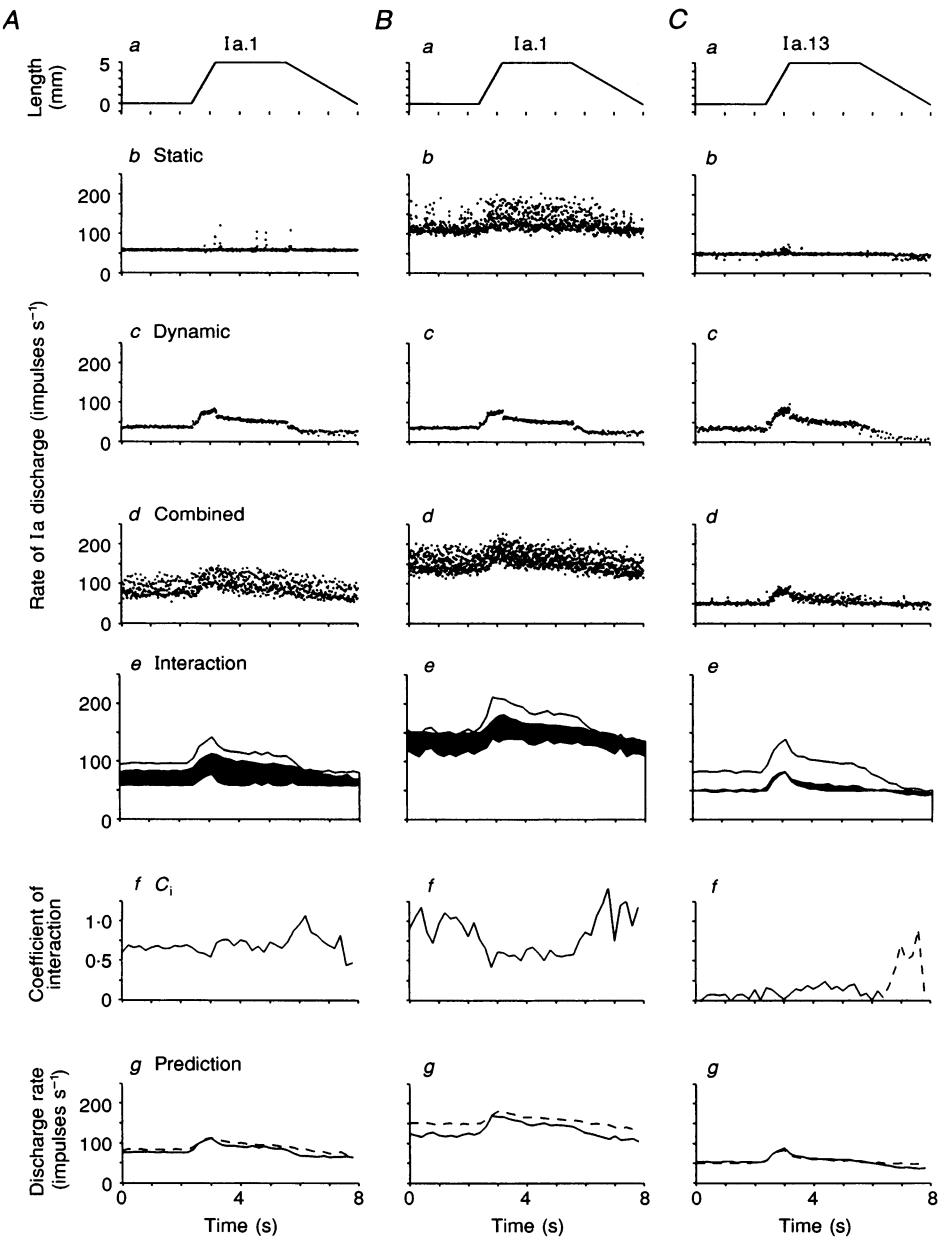

Figure 3. Individual Ia responses during stretch

Responses of individual Ia afferents that showed overall high (Ia.1, *A* and *B*) or low (Ia.13, *C*) values of C_i. *a*, muscle length; *b–d*, responses, shown as plots of instantaneous discharge rate, during static (*b*), dynamic (*c*), and combined static and dynamic (*d*) fusimotor stimulation; *e*, a graphic representation of the amount of summation between the presumed separate static and dynamic encoding sites; *f*, coefficient of interaction, computed in 200 ms bins; *g*, an empirically derived prediction of the combined response (continuous line) compared with the actual response (dashed line), the prediction being based on the separate responses during static and dynamic stimulation, and the corresponding afferent preterminal-branch tree (see Discussion and eqn (3)). The traces in *e* are mean firing rates with the interaction band shown by the filled area. This is the difference between the response to combined stimulation (middle trace) and the momentarily greater response to either static or dynamic stimulation alone (bottom trace). Comparison of the interaction band with the difference between the linear sum of the separate responses (top trace) and the response to combined stimulation gives a visual impression of the amount of summation present throughout the stretch cycle. Stimulation rates of the fusimotor axons (in impulses s^{-1}): static (rows *b* and *d*), 60 (*A*), 110 (*B*), 100 (*C*); dynamic (rows *c* and *d*), 125 (*A* and *B*), 100 (*C*). Note 1 : 1 driving by the static axon in *A* and 1 : 2 driving in *C*, indicating extensive chain fibre activity in each case. Calculation of C_i (row *f*) and predicted discharge rates (row *g*) based on probability density estimates of discharge rates calculated over consecutive bins of 200 ms duration.

it was clearly not attributable to any non-stationarity of Ia responses or fusimotor action (such as intrafusal fatigue), since, when present, it was highly reproducible in successive measurements, and the effects seemed sufficiently specific to merit modelling studies (see Model simulations). In order to illustrate the phenomenon more convincingly, the responses which showed it most clearly were selected and averaged. The resulting subpopulation responses are displayed in Fig. 5, for combinations tested either with modulated static (Fig. 5*A*) or modulated dynamic (Fig. 5*B*) action (4 combinations in

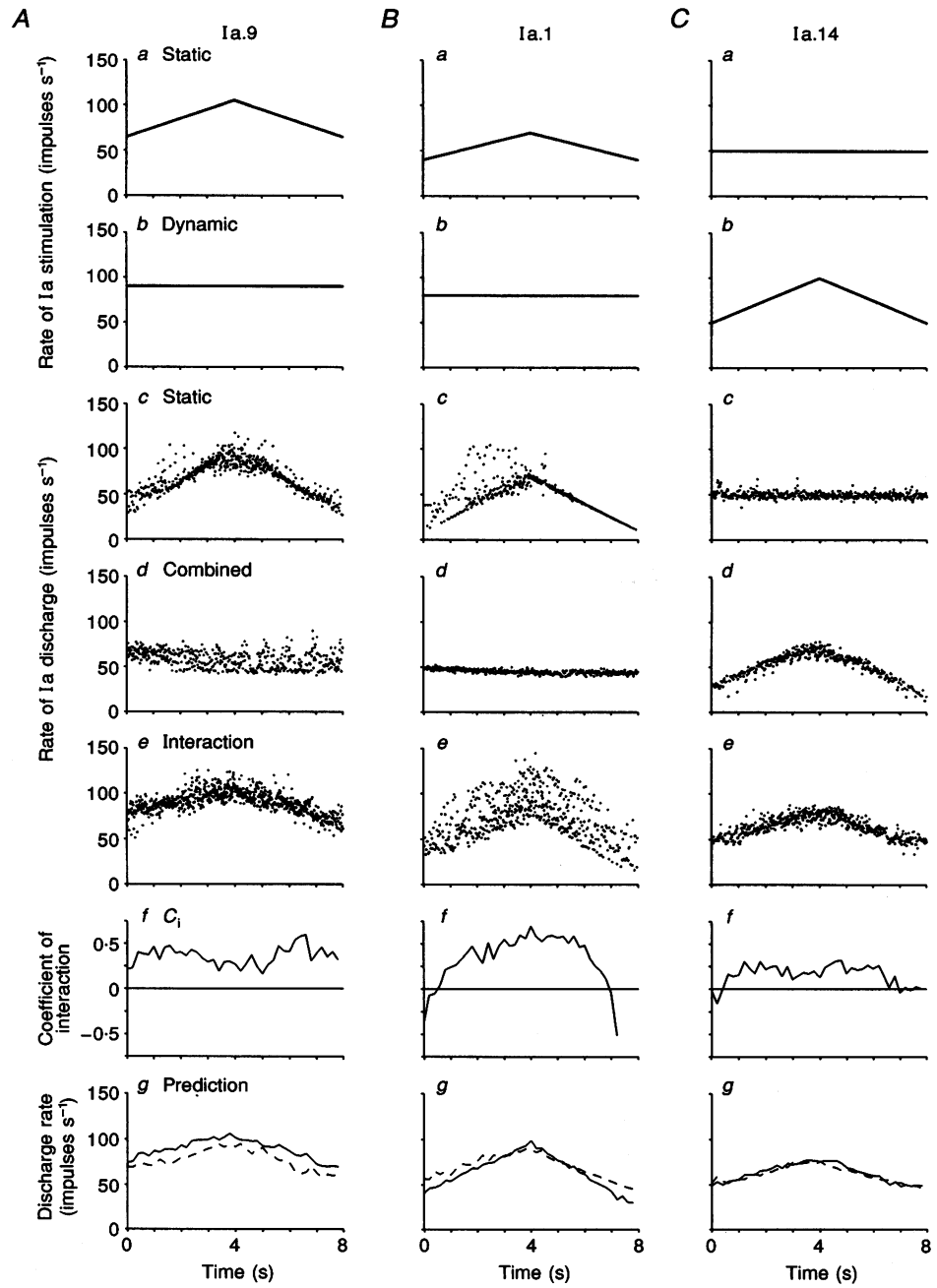

Figure 4. Individual Ia responses at constant length

Responses of individual Ia afferents while the muscle was held at constant length; one fusimotor axon was stimulated at a triangularly modulated rate (static, *A* and *B*; dynamic, *C*), and the other was stimulated at a constant rate. *a*, static and *b*, dynamic fusimotor stimulation rates; *c–d*, responses to separate static (*c*) and dynamic stimulation (*d*), and to combined static and dynamic stimulation (*e*), shown as plots of instantaneous discharge rate; *f* and *g*, same arrangement as Fig. 3. Note that C_i varies during the stimulation protocol (T3), tending to show maximum values when the separately evoked responses are about equal, irrespective of which input was modulated (static, *A*; dynamic, *C*). Also shown is an example of the phenomenon we have called hyperocclusion (*Bf*, afferent Ia.1), in which C_i is negative and which is described fully in the text (see also Fig. 5).

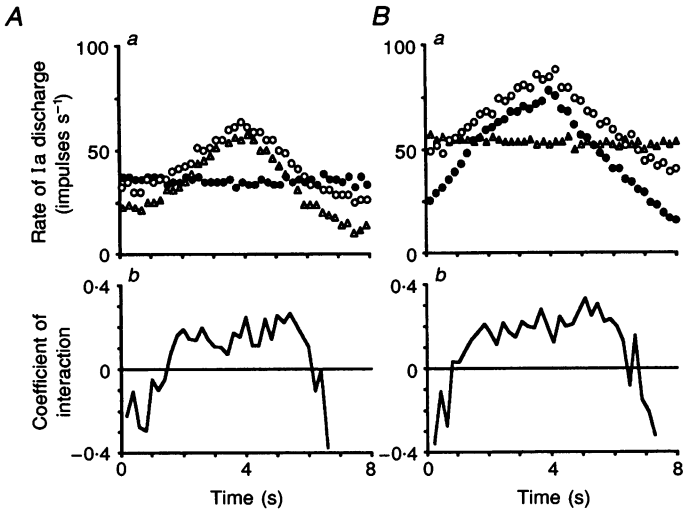

Figure 5. Averaged Ia responses revealing hyperocclusion at constant length

Population responses of subsamples of Ia afferents that showed some degree of hyperocclusion during fusimotor stimulation at constant length. The responses were averaged using probability density estimates of discharge rate (200 ms bins). Hyperocclusion was seen during modulation of either the static (*A*) or dynamic (*B*) input. *a*, population responses to separate static (△) and dynamic (●) stimulation, and to combined static and dynamic stimulation (○). *b*, coefficient of interaction. In each case (*A* and *B*) data from four separate combinations of a Ia afferent together with a static and a dynamic efferent were averaged, from an overall total of seven such combinations, one being common to both *A* and *B*. For full details see text.

each case). The features described above for individual responses were clearly confirmed. Thus, it can be seen that for rate-modulated stimulation (both single-fibre and combined action) the carrier rate tended to decline over the 8 s stimulation period, as discharge rate at the end of the cycle was well below that at the beginning of the cycle, while discharge rate adaptation during stimulation at constant rate was negligible. Therefore, with discharge during combined action only slightly above the levels of single-fibre action at the beginning of the cycle, appreciable adaptation of discharge rate during combined action could easily lead to the condition of $R_c < R_n$ towards the end of the stimulation cycle, leading to a sharp decline and negative values of C_i (Fig. 5*A b* and *B b*). The fact that C_i values could also be negative at the beginning of the 8 s cycle seems to be at variance with this explanation, but in

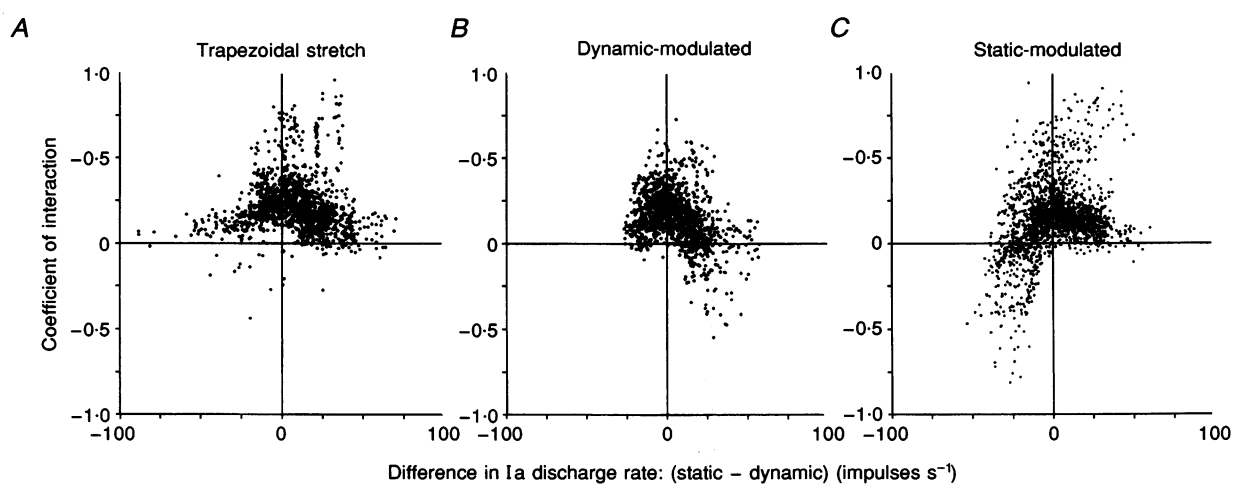

Figure 6. Dependence of C_i on difference between separately evoked responses

The dependence of coefficient of interaction (C_i) on the difference between the static- and dynamic-evoked Ia discharge rates. Individual points are calculated from 200 ms bins. Data are included from all combinations that were studied of a Ia afferent together with a static and a dynamic efferent. Note that C_i tends show to a maximum value when the separately evoked discharge rates are the same, a phenomenon shown both during trapezoidal stretch (protocol T1, *A*) and with the muscle at constant length (protocol T3) when either the dynamic (*B*) or static (*C*) input was modulated.

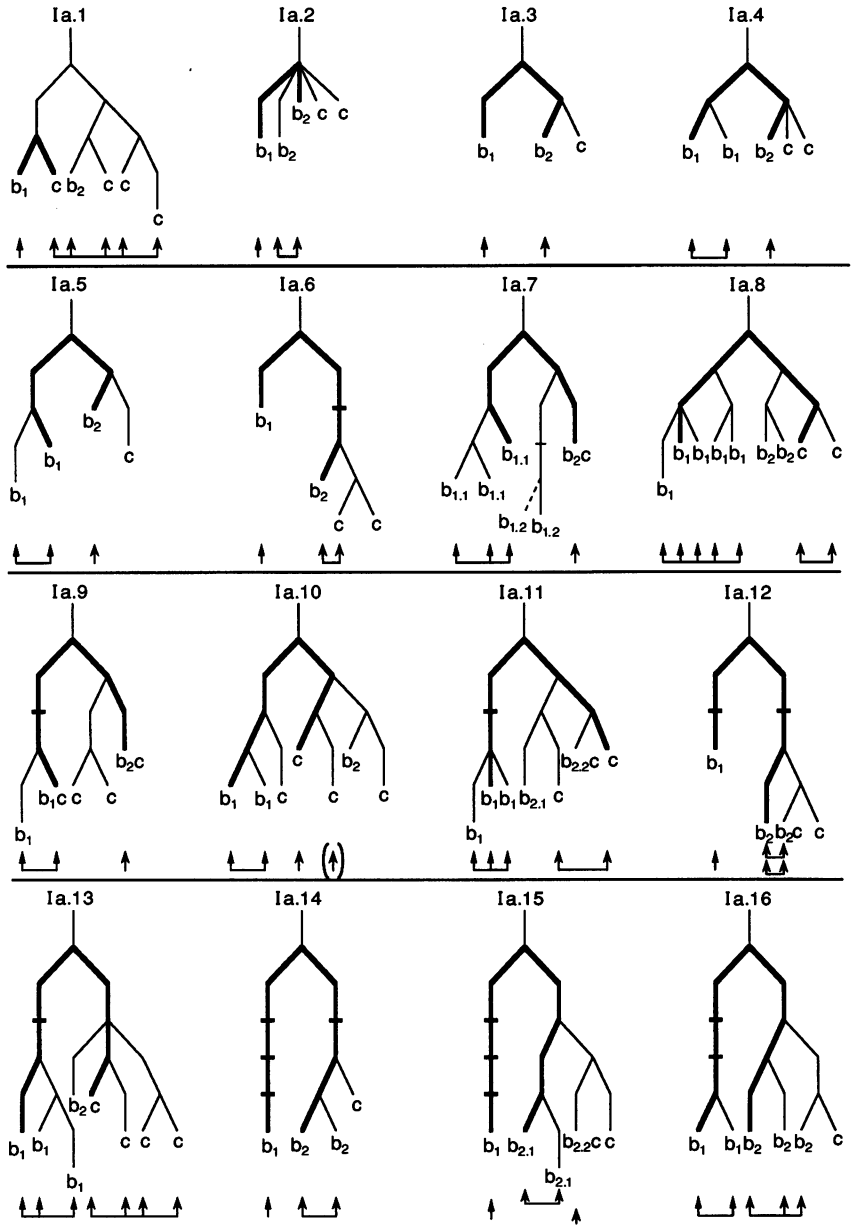

Figure 7. Topology of Ia preterminal branches

Schematic diagrams showing the topology of the myelinated preterminal branch trees of all 16 Ia afferents reconstructed from serial sections. Nodes of Ranvier are indicated as branch points, inflexions, or as short horizontal lines, with the special case of heminodes being shown as the free ends of the ultimate preterminal branches. Unmyelinated preterminal branches arising from the heminodes are not included, but their intrafusal distributions are shown as follows: b_1, bag_1 fibre; b_2, bag_2 fibre alone; c, chain fibre(s) alone; b_2c, both bag_2 and chain fibre(s) together. It should be noted that the number of preterminal branches distributed to particular types of intrafusal fibre does not in general correspond to the number of each type present (see Banks, 1986). The dashed line in the tree of afferent Ia.7 represents the only example of an unmyelinated branch arising from a complete node. The number of chain fibres varied from 3 to 6; when two bag fibres of the same type were present, they are indicated separately as $b_{n.1}$ and $b_{n.2}$, where n identifies the type. The vertical arrows below each tree indicate the inferred dynamic (to b_1) and static (to b_2, c, or b_2c) inputs; they are coupled whenever more than one input would have been simultaneously active, in some cases due to intrafusal branching of the fusimotor axon. However, not all possibilities of fusimotor inputs have been included; whenever alternatives existed the one shown is that which involved the shortest path between the inputs, as measured by the number of complete nodes present in it. The MPL is marked by a thick line in each tree. Alternative inputs are exceptionally included for afferents Ia.10 (arrow in brackets indicates the static input preferred on histological evidence), and Ia.12 and Ia.15 (double rows of arrows emphasize that different combinations of inputs were used, see also Table 1). Note that MPL varies from 1 (afferent Ia.1) to 9 (afferents Ia.14–Ia.16), and that the afferent trees are arranged in order of increasing values of MPL. Note also that individual responses of Ia.1, Ia.9, Ia.13 and Ia.14 are illustrated in Figs 3 and 4, and that simplified versions of the branch trees of afferents Ia.1 and Ia.13 were used for the computer simulations of Fig. 10.

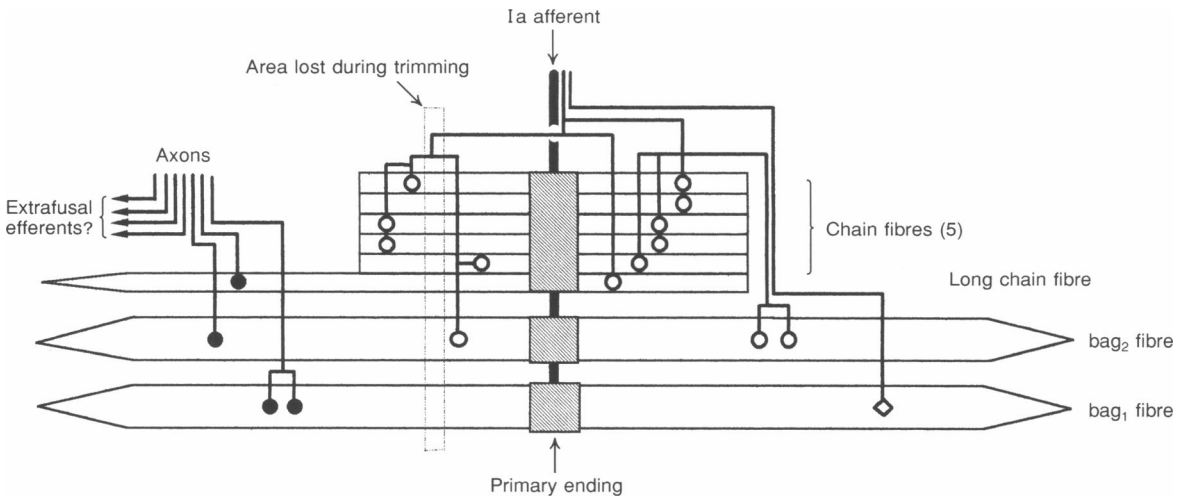

Figure 8. Schematic representation of the innervation of spindle 266/2

Diagram is based on a reconstruction from 1 μm serial sections (cf. Table 1). A small portion (inferred) was lost during block trimming. This spindle contained the sensory ending of afferent Ia.1 (see Fig. 7 for tree topology). The motor innervation is supplied by 5 axons, 3 of which possess features indicating that they are intrafusal branches of β-axons (intrafusal endings indicated by ●). Of the remaining 2 axons, one to a single pole of the bag_1 fibre, and the other to both poles of the bag_2 and most of the chain fibres, may be identified with the dynamic (ending indicated by ◇) and static γ efferents (endings indicated by ○), whose effects are shown in Figs 3 and 4*B*.

order to permit analysis of steady-state responses, the first full cycle of stimulation (as shown in Fig. 5) was preceded by 2 s of stimulation (see Methods, Fig. 1), which elicited transient initial peaks of discharge comparable in magnitude to those provoked by rate-modulated stimulation (not illustrated and not analysed in detail). Therefore, at the beginning of the illustrated response cycles a certain amount of firing rate adaptation was most probably already present.

Plotting values of C_i against the difference between the separate responses evoked by static and dynamic stimulation for individual 200 ms sampling bins clearly demonstrates both the occurrence of hyperocclusion and the dependence of C_i on the difference between the discharge rates of the separate static and dynamic responses (Fig. 6). The tendency for maximum values of C_i to be attained at zero difference was present during trapezoidal stretch (Fig. 6*A*) as well as at constant length (Fig. 6*B*, dynamic input modulated; and Fig. 6*C*, static input modulated), with most values clustered between 0·0 and 0·5 in each case. In contrast, hyperocclusion was developed reproducibly only when the muscle was held at constant length. As with positive values of C_i, the size of negative values of C_i depended in a similar manner on the difference between static- and dynamic-evoked responses, becoming more negative with increasing difference.

The variability of C_i according to phase of muscle stretch and conditions of motor stimulation not only complicates the quantitative comparison of spindle primary endings but also raises the possibility that factors additional to encoding site interaction are involved in determining the overall primary output. Such factors would be expected to vary quite independently of encoding site interaction and, if of sufficient magnitude, to lead to independent shifts in the relative values of C_i when the same endings are tested under different conditions. That this is, in fact, not so is shown by the subsample of our data analysed in Table 1*B*. The data were derived from the largest group of spindles each of which had been tested using a comparable set of three different stimulus conditions (bold data in Table 1*A*). Mean values of C_i were computed from sampling bins where the discharge rates elicited by separate static and dynamic stimulation differed by < 10 impulses s^{-1}. This criterion was chosen as a compromise between the need to minimize the artifact arising from the dependence of C_i on discharge rate difference and the need to retain sufficient data for adequate quantitative comparison (see Fig. 4). For the seven spindles concerned, the values of C_i obtained under the different conditions are very highly correlated, indicating that when suitably constrained the value of C_i is characteristic for each primary ending.

Topological structure of Ia myelinated preterminal branches

The topological structures of the myelinated preterminal branches were successfully reconstructed for sixteen of the primary endings whose positions had been marked after recording the results of at least one stimulus protocol in each case. The main findings are illustrated in the schematic summaries of each afferent's preterminal-branch structure of Fig. 7. Branching necessarily occurs at nodes of Ranvier, though not all nodes within the preterminal trees are branched. Considering the trees to begin at the first

branched node of the parent Ia afferent, each tree contained between three and fourteen complete nodes (that is, those flanked on both sides by myelinated segments). Out of a total of 130 complete nodes sixty-five were branched, the proportion for individual endings varying from 4/13 (30%) to 3/3 (100%). These two properties of the trees showed no correlation, but in each case much of the variability appeared to be associated with individual animals. Thus, the mean number of nodes per ending per cat ranged from 4·5 to 10·5, and, quite independently, the mean proportion of branched nodes per ending per cat ranged from 34 to 78%.

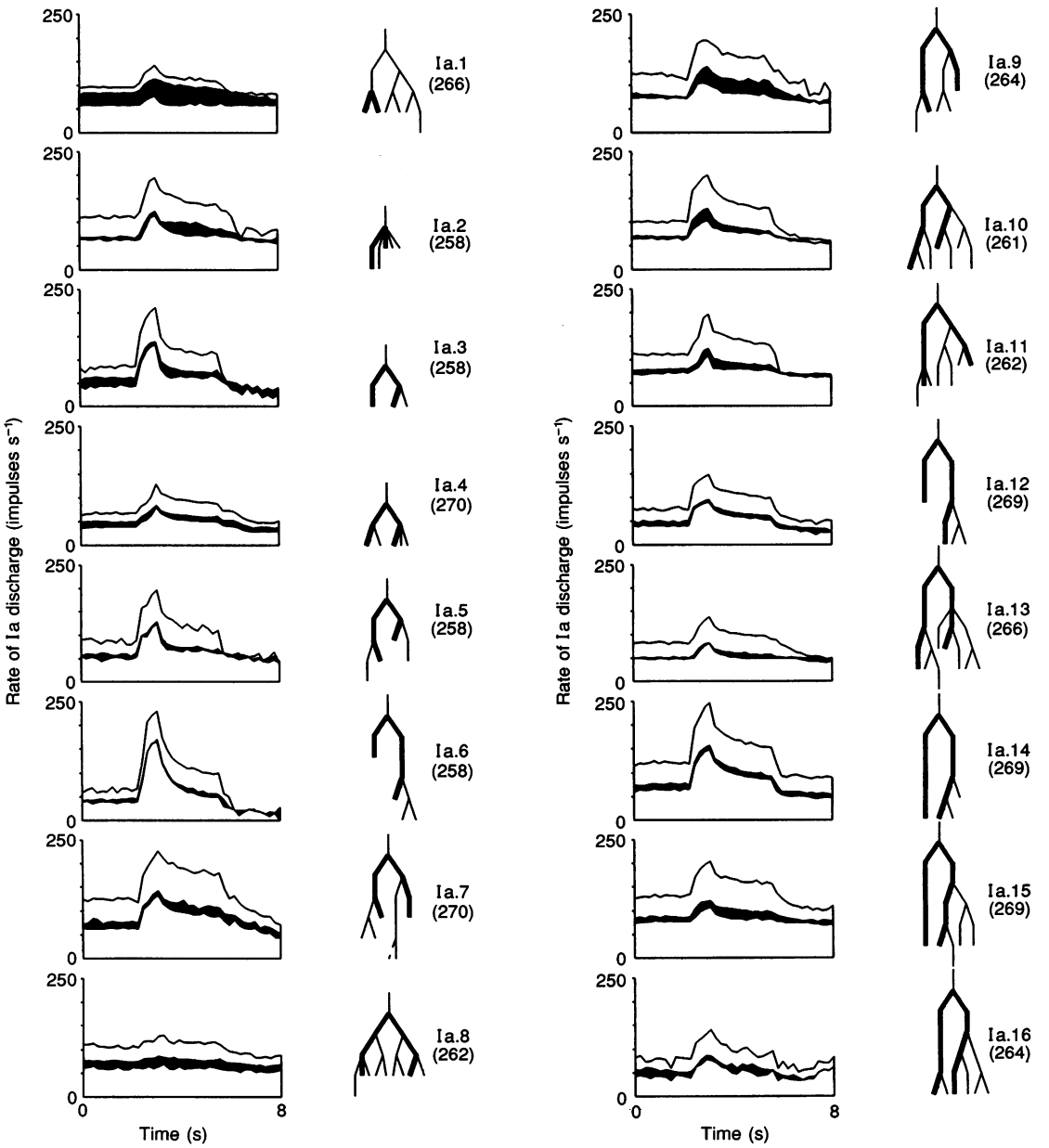

Figure 9. Comparison of pacemaker interactions of putative encoding sites with minimum path length between them

Visual comparison of the amount of interaction between static- and dynamic-evoked responses during trapezoidal stretch, as assessed by interaction bands (filled black bands, see Fig. 3), with the corresponding Ia afferent tree topology. The afferents are identified by number alongside reduced versions of their topologies, as given in detail in Fig. 7. These in turn are presented alongside averaged responses (bin width, 200 ms) of the same format as given in Fig. 3*Ae* and *Be*. Stimulation rates were 100 impulses s^{-1} for both the static and the dynamic axons in all cases except Ia.1 (static, 60 impulses s^{-1}; dynamic, 125 impulses s^{-1}) and Ia.4 (static, 120 impulses s^{-1}; dynamic, 120 impulses s^{-1}). The dynamic axons to Ia.8, 9, 10, 11 and 16, and the static axon to Ia.10, were β-axons. Spindles derived from the same muscle are identifiable by the experiment numbers given in parentheses.

In spindle primary endings, branching at complete nodes is typically dichotomous, and daughter branches are all normally myelinated (Banks *et al.* 1982; Banks, 1986). In the present sample sixty nodes branched dichotomously, four trichotomously (Ia.4, Ia.8, Ia.11 Ia.13 in Fig. 7), and one pentachotomously (Ia.2, Fig. 7); exceptionally, one of the daughter branches of a dichotomous node was unmyelinated (Ia.7). Of the eighty-six ultimate myelinated segments that resulted, thirty-one (36%) were distributed to bag_1 fibres, nineteen (22%) to bag_2 fibres, twenty-eight (33%) to chain fibres, seven (8%) to both bag_2 and chain fibres, and one (1%) to both bag_1 and chain fibres. Most endings possessed a first-order branch supplied exclusively to a single bag_1 fibre (for instance Ia.4–Ia.6 in Fig. 7), as is typical of primary endings in tenuissimus. In one spindle two bag_1 fibres were present (Ia.7), one supplied exclusively by a first-order branch, the other by a second-order branch whose parent also supplied the bag_2 and chain fibres. In two spindles (Ia.1 and Ia.10) a single bag_1 fibre received an exclusive distribution only from a second-order branch whose parent also supplied either one or several chain fibres. Finally, in one spindle (Ia.9) the sensory terminals of the single bag_1 and one of the four chain fibres shared a common heminode on a second-order branch.

Since the terminals ultimately derived from the preterminal branches are separate from each other (Banks, 1986), the

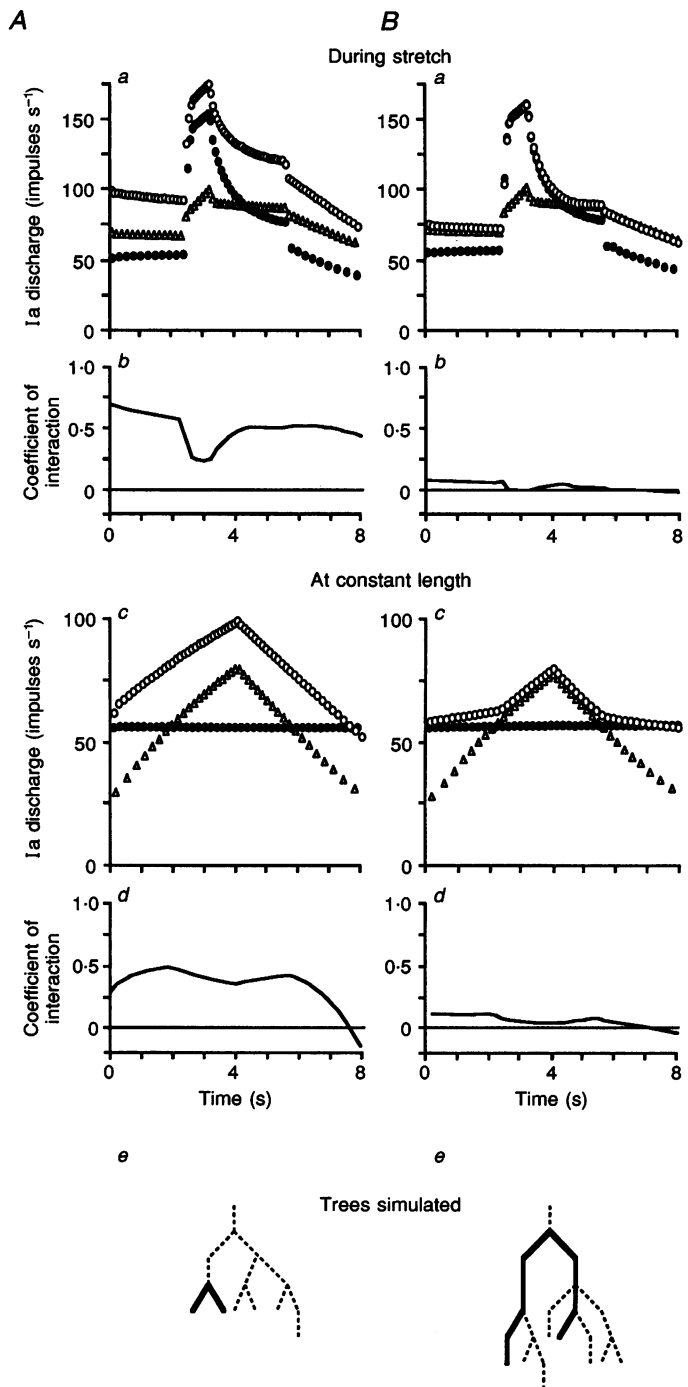

Figure 10. Model Ia responses during stretch and at constant length

Simulated responses (*a* and *c*), together with the corresponding coefficients of interaction (*b* and *d*), of afferents with minimum path lengths of 1 (*A*) and 8 (*B*). The simulations were generated using a combined mechano-ionic model as described in the Methods. Responses are shown to both trapezoidal stretch with constant fusimotor input(s) (*A a* and *Ba*), and at constant muscle length with triangularly modulated static fusimotor input, or constant dynamic fusimotor input, or both (*A c* and *Bc*). ●, dynamic fusimotor input active alone; △, static fusimotor input active alone; ○, response during combined stimulation. Note the generally high values taken by C_1 when MPL is 1 (*A b* and *d*), as compared with the low values when MPL is 8 (*B b* and *d*), and the appearance of hyperocclusion following the high discharge rates evoked during combined fusimotor stimulation in *A c*. For further details see text. The trees simulated are those of the minimum interaction paths of afferents Ia.1 and Ia.13, whose simplified representations are shown in *A e* and *Be*, respectively, and some of whose responses to trapezoidal stretch and at constant muscle length are shown in Figs 3 and 4*B*.

dynamic and static encoding sites must interact via the preterminal tree. Taking into account the nature of the static-induced responses, so as to infer whether the bag_2 or chain fibres (or both) were active (see Methods), it is possible to determine the shortest path for encoder interaction in each ending (thick lines in Fig. 7). We shall refer to the number of complete nodes in this path as the minimum path length (MPL), which can be seen to range from 1 to 9 (corresponding to 2–10 myelinated segments, or internodes). It should be noted that in most endings identification of the probable static effector makes either no difference or a difference of only 1 to the value of MPL. This was also true for the spindle with two bag_1 fibres (Ia.7), where either could be the dynamic effector, without this ambiguity altering the value of MPL. However, the evidence for the particular shortest interaction paths shown in those trees where bag_1 is supplied exclusively by only a second-order branch (Ia.1 and Ia.10), or not at all (Ia.9), needs to be critically examined, since incorrect identification of the active static encoder nearest to the bag_1 fibre would seriously affect MPL in these cases.

The static action of Ia.10 was elicited by a β-axon. Typically, though not invariably, β-axons innervate the long pole of a long chain fibre, and this pole does not normally receive γ innervation (Banks, 1994*b*). The spindle containing afferent Ia.10 was sectioned longitudinally so as to include the juxta-equatorial regions where γ innervation of chain fibres occurs. There were five chain fibres, all of which received motor endings in one juxta-equatorial region whereas only four received them in the other. These four fibres therefore were almost certainly not innervated by the static β-axon. The first-order branch of the Ia afferent to the bag_1 fibre was also directly distributed to one of these, but did not appear to be distributed to the remaining chain fibre, which was almost certainly the only one activated by the static β-axon. The MPL is therefore shown as 6 rather than 3.

In the case of Ia.1, where the static action was elicited by a γ-axon, 3-dimensional graphic reconstruction demonstrated clearly that one of the six chain fibres did not receive primary sensory terminals from the Ia first-order branch that was distributed to the bag_1 fibre. All six chain fibres also received sensory terminals from the other first-order branch, so the MPL could be either 1 or 5 in this case. It was therefore particularly important to establish as completely as possible the pattern of motor innervation in this spindle. The motor axons entered the spindle in two nerves, one the main spindle nerve containing the only afferent axon, the second a small branch of what appeared to be an otherwise exclusively extrafusal motor nerve, though this could not be confirmed due to teasing damage. This latter nerve contained three intrafusal motor axons whose route to the spindle, and the form of whose endings, strongly indicated that they were β-axons (Banks, 1994*b*). They supplied the bag_1 fibre, the bag_2 fibre, and the long pole of a long chain fibre, which was the only chain fibre definitely not to receive sensory terminals from the Ia first-order branch to the bag_1 fibre. The main spindle-nerve itself contained only two motor axons, both presumably γ-axons. One supplied the distal pole of the bag_1 fibre alone, whereas the other supplied both poles of the bag_2 fibre, the distal poles of all six chain fibres, and the proximal poles of at least four of the chain fibres (Fig. 8). The extensive chain fibre distribution of this axon is, of course, commensurate with its driving action on the primary ending (Figs 3 and 4), and would have ensured that the static input to the bag_1/chain first-order branch of the Ia was activated, giving the MPL a value of 1.

A γ-axon also elicited the static action of Ia.9, an action diagnosed as due to both bag_2 and chain activation, whereas the dynamic effect was due to a β-axon. Reconstruction of the motor innervation of the spindle was therefore again essential since the occlusion seen during combined static and dynamic stimulation (Table 1 and Figs 4 and 9) could not be explained by the present model of pacemaker interaction if the static axon were to supply the particular chain fibre whose terminals shared a second-order heminode with those of the bag_1. There proved to be only two candidate static γ-axons, one in each pole. They supplied the bag_2 and either two or three of the chain fibres, but neither of them innervated the chain fibre of immediate interest. Thus MPL could not be zero for the particular combination of static and dynamic axons concerned, but rather must be 6.

Comparison of pacemaker interaction and tree topology

There are several features of afferent tree topology that could conceivably influence encoding site interaction, on the assumption that all heminodes are potential pacemakers. These include the number of terminal branches, the total number of nodes and heminodes, the proportion of branched nodes in the complete tree (for all of the above, if they acted as sinks of generator currents from remote transducer sites), and the MPL, which has been defined above. The only such feature for which we have any clear evidence of involvement in pacemaker interaction is MPL.

The sixteen successfully reconstructed afferent trees, arranged according to increasing values of MPL, are shown in simplified form in Fig. 9. Each one is presented alongside an interaction band version of its responses to trapezoidal stretch during dynamic, static, and combined stimulation. The predominance of interactions with high degrees of occlusion is clearly shown in these plots. Values of C_i for each ending, obtained under various stimulus conditions, are compared with the corresponding values of MPL in Table 1*A*. In each case C_i was calculated as the mean of the individual data from those sampling bins where the discharge rates elicited by separate static and dynamic stimulation differed by < 10 impulses s^{-1}. A complete series was obtained only for trapezoidal stretch, but the full range of values of MPL was also covered by the high overall discharge rate responses when the muscle was held at constant length during either dynamic or static modulation. Spearman's rank correlation coefficient for these three series ranged from $-0{\cdot}37$ to $-0{\cdot}73$, and of these the two higher

values were statistically significant (Student's t test, Table 1C).

Model simulations

Simulations were carried out on simplified trees based on the tree topology of afferents Ia.1 and Ia.13, which had MPL values of 1 and 8, respectively. The simplified trees are those shown by the thick lines in the icons of Fig. 10Ae and Be (same structure as in Fig. 7; dashed lines indicate the segments of the tree that were not simulated). The simplification of the tree structure was motivated by preliminary studies which demonstrated that, in simulations, MPL was by far the most influential factor determining pacemaker interaction (see below), and that even large configurations of branching fibres collaterally appended to the shortest path had only negligible effects (K. A. Scheepstra, E. Otten & M. Hulliger, unpublished observations).

Comparison of Fig. 10Aa and Ba with the population responses of Fig. 2 shows that the current version of the model adequately simulated several of the key features of static and dynamic fusimotor actions on Ia responses to trapezoidal stretch, including the major effects on sensitivity to imposed movements, the occurrence of a slow decay of Ia discharge (after a ramp stretch) due to dynamic action, and (true for tenuissimus but not for all muscles) the persistence of maintained discharge during muscle shortening in the presence of both static and dynamic action. Similarly, the comparison of Fig. 10Ac and Bc with the averaged responses of Fig. 5 illustrates that the main features of Ia responses to tonic and modulated fusimotor stimulation at constant length were reproduced satisfactorily. Furthermore, the simulated responses to combined static and dynamic activation also revealed some of the principal features of C_i, as observed experimentally. Thus C_i values revealed local minima when the difference between statically and dynamically induced discharge was largest (especially manifest in Fig. 10Ab and Bb), and local maxima, when the difference was minimal (clearly seen in Fig. 10Ad and Bd). However, the main question addressed was whether simulations of different path lengths between static- and dynamic-operated encoding sites would produce significant effects on the coefficient of interaction.

The real primary ending of Ia.1 consistently showed the greatest values of C_i of any primary under comparable circumstances, whereas that of Ia.13 typically showed the least values (Table 1). The results of the simulations support the notion that this difference of behaviour can largely be attributed to differences in MPL. For small values of MPL (Fig. 10A) values of C_i were high (ranging between 0·25 and 0·7), comparable with those observed experimentally for Ia.1. In contrast, simulations with an MPL of 8 led to values of C_i (below 0·1) which were as small as those seen experimentally for Ia.13. In addition, it should be noted that simulations of the highly summating ending of Fig. 10A successfully revealed a phase of hyperocclusion at the end of the protocol combining constant length with triangularly modulated static and constant rate dynamic stimulation (Fig. 10Ad), while failing to do so in the responses to trapezoidal stretch during constant rate activation of both types of efferent (Fig. 10Ab). Similar general trends were seen for simulations of the occlusive ending of Fig. 10B, although on a smaller scale. It may also be noted that, in the case of high MPL values, spurious indications of hyperocclusion could be observed in simulated responses to trapezoidal stretch, in line with the experimental observation of rare instances of negative values of C_i under those conditions (cf. Fig. 6A and see Methods).

It must be emphasized that hyperocclusion could only be simulated with the version of the model featuring an added hyperpolarizing process with a very long time constant; as described in the Methods, this was implemented by simulating a voltage-dependent K^+ conductance with very slow activation characteristics. The main influence of this channel was to induce appreciable discharge rate adaptation during and after episodes of discharge above approximately 50 impulses s^{-1}. The phenomenon was especially evident at lower discharge rates, due to a steeper current–rate relation in this domain (see Otten *et al.* 1995*a*). Thus, for the rates typically seen during stimulation at constant length, adaptation effects occurred on a significant scale only in simulations of combined static and dynamic action, allowing the discharge rate at the end of a triangle cycle to fall below the momentary R_h value, which on its own was not subject to significant adaptation (Fig. 10Ac). In contrast, simulations of the higher discharge rates (during separate static and dynamic stimulation), as seen experimentally in responses to large trapezoidal stretch, revealed significant adaptation at the end of the trapezoidal cycle in both static- and dynamic-induced responses. This precluded that discharge during combined activation (R_c), which, on its own, revealed only moderately larger adaptation (see above), fell below the self-adapted value of R_h (Fig. 10Aa). Finally, since manifestation of hyperocclusion depended on firing during combined activation being significantly more adapted than during single-fibre activation (R_h), it should be more pronounced when R_c was augmented due to partial summation in trees with short MPL (Fig. 10Ac), compared with trees with longer MPL, where R_c was practically identical with R_h (Fig. 10Bc). Comparison of Fig. 10Ad with Bd shows that this indeed was the case.

In summary, the computer simulations confirmed that preterminal-branch topology can influence the degree of occlusion between inputs operating separate encoding sites, that summation (due to electrotonic spread of receptor current) was largely determined by the separation of these encoding sites, and that hyperocclusion could be accounted for by discharge rate-dependent ionic adaptation. It also demonstrated that the preferential manifestation of hyperocclusion at constant length was largely fortuitous, if discharge rate-dependent adaptation was operative for all but the lowest discharge rates.

DISCUSSION

The mechanism of occlusion

The occlusion seen during combined stimulation of one fusimotor action by another that is momentarily more effective when each acts alone has usually been explained as due to the existence of separate encoding sites associated in particular with the dynamic and static inputs to the Ia afferent (Lennerstrand, 1968; Hulliger *et al.* 1977; Hulliger & Noth, 1979). Each encoder is thus potentially able to act as, or to entrain, the final output pacemaker of the Ia axon, and to occlude the other by antidromic invasion and resetting.

In principle occlusion (i.e. strongly sublinear summation of responses to separate stimuli) could be a formal manifestation of non-linear receptor properties, with gain-compression characteristics producing simple saturation of discharge rate. There is little doubt that the receptor as a whole has striking non-linear properties (reviewed in Hulliger, 1984; Hunt, 1990). However, for the present consideration the only issue is whether gain compression in the discharge rate–current relation of a single encoding site could account for the degree of occlusion seen during combined activation of separate fusimotor fibres, since any gain compression in discharge rate–length or –tension relations, arising from non-linearities in transducers and mechanical filters must have been present to the same degree during separate and combined activation of fusimotor fibres. Three lines of evidence argue against the possibility of occlusion being largely due to encoder saturation. First, in reviewing the observations from isolated mammalian spindles, Hunt (1990) concluded that the discharge rate–current relation of the encoder was largely linear. The argument rested on the similarity of compound receptor potential and discharge rate profiles in response to identical stimuli, but did not explicitly address the effects of possible competitive interaction of multiple encoding sites on discharge patterns. Second, cat spindle afferents are capable of discharging at rates up to 500 impulses s^{-1} (see Hulliger, 1984 for review), well above the peak discharge rates of around 200 impulses s^{-1} of the present responses (see Figs 2–5 and 11). Arguably, tenuissimus spindle afferents might have a more limited range of discharge rates, but the more parsimonious explanation is that mechanical constraints preclude application of sufficiently large stretches to activate them over the entire range of possible discharge rates. Third, several observations on the present interaction experiments clearly indicate that low values of C_i were found well below, and that they were largely independent of, peak discharge rates: comparison of the responses of Fig. 3*A* and *B* shows that in the case of afferent Ia.1 mean C_i if anything increased (i.e. summation, rather than occlusion, was augmented) when mean discharge rate during combined activation was doubled. Finally, scatter plots and regression analysis of C_i *vs.* absolute discharge rate during combined stimulation (Fig. 11*A*, same data as in Fig. 6) failed to reveal a significant negative correlation.

Could occlusion simply arise from mutual mechanical unloading of statically and dynamically operated intrafusal fibres? Limitations of current methods probably preclude a definitive answer, since direct measurements in isolated spindles of both length changes and tension transients of

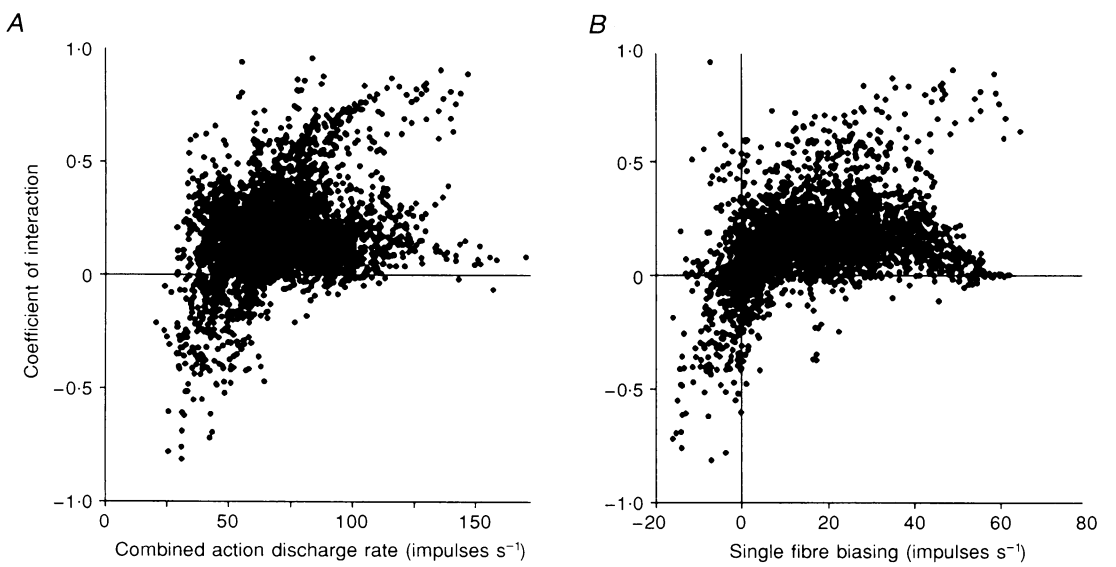

Figure 11. Evidence that occlusion is not due encoder saturation (*A*) or to mutual intrafusal fibre unloading (*B*)

Scatter plots of C_i against combined static- and dynamic-evoked discharge rate (*A*), and against the increase in discharge rate (biasing) evoked by individual fusimotor axons (*B*), show no overall negative correlation, in contrast with what would be expected if saturation or mutual unloading occurred. Each point is calculated from a 200 ms bin.

individual intrafusal fibres would be required. However, the observations of Fig. 11*B* seem to rule out that unloading could be the predominant cause of occlusion, since, in general, unloading effects could be expected to be most significant when single-fibre action (as estimated by the amount of biasing) was most powerful. Yet the scatter plot of C_i *vs.* single-fibre biasing strength again failed to reveal the predicted negative correlation (Fig. 11*B*, same data as in Figs 6 and 11*A*), although it could be argued that for a subsample of data points (lower cluster for large bias values) a trend that might indicate very weak unloading could be identified. The manifestation of formally negative biasing effects in Fig. 11*B* is most parsimoniously attributed to firing rate adaptation (mainly towards the end of trapezoidal stretch), following transients of high discharge rate during dynamic stretch (see below).

The phenomenon of hyperocclusion, which was encountered when fusimotor axons were stimulated at constant length, was an unexpected observation. Possible mechanisms were explored in computer simulations. The main conclusion was that a significant component could be attributed to a process of slow adaptation, formally simulated as a very slowly activating K^+ conductance. As pointed out in the Results, this is by no means a unique interpretation, as other hyperpolarizing processes could easily lead to the same kind of slow adaptation behaviour. Alternatively mutual mechanical unloading of static- and dynamic-operated intrafusal fibres might also contribute to the phenomenon, but an exclusively mechanical explanation would certainly be less general, since it is not immediately evident why such unloading should almost exclusively occur at constant length, while being virtually absent during imposed movement.

The reality of separate static and dynamic encoding sites

The phenomenon of occlusion is thus a compelling reason to suppose that separate encoding sites associated with the static and dynamic inputs do usually exist. However, this has been denied by Kröller, Grüsser & Weiss (1990) who carried out a statistical analysis on the discharge patterns of Ia afferents of passive spindles during steady stretch with or without near-threshold random modulation. Kröller *et al.* assumed that the response to the velocity component of the stretch was due entirely to the bag_1 fibre, whereas the response to the static component was assumed to be due to the bag_2 and chain fibres. It is clear, however, that these assumptions are unjustified, especially perhaps in the passive spindle, since all muscle fibres will have some dynamic properties. Indeed it has been shown by Price & Dutia (1989) that spindles possessing only bag_2 and chain fibres do show dynamic responses, though of course these cannot be enhanced by dynamic fusimotor input. It has also been argued that the resting discharge of the passive spindle with a full complement of intrafusal fibres does not arise from sensory terminals on the bag_1 fibre (Gioux, Petit & Proske, 1991). Thus it seems likely that under the conditions of the experiment of Kröller *et al.* the output of the Ia afferents was in fact being determined principally by a single encoding site, possibly one associated with the bag_2 fibres. Carr, Morgan & Proske (1996) recently postulated that an encoding site associated with the bag_2 fibre can be specifically activated by succinyl choline, and they demonstrated mutual occlusion of this activity and that elicited by simultaneous dynamic γ stimulation.

In the case of the tendon organ, Fukami (1981), using an isolated preparation from the cat tail, was also unable to demonstrate the presence of more than one encoding site in each receptor. However, the direct stimulation of extrafusal muscle fibres and the electrical depolarization of the afferent axon that Fukami employed would almost certainly have similarly and simultaneously affected any encoding sites present, such that the intrinsically most excitable would become tonically active. Combination of the two stimulation methods would be expected to enhance that excitability further, leading to the observed summation of effect. In contrast, Gregory *et al.* (1985) used ventral root stimulation to activate single motor units in cat soleus and observed various degrees of occlusion (or non-linear summation) of the response to one motor unit by that of another acting on the same tendon organ. By comparing their results with simulations derived from models having either separate parallel or single central encoders they were able to conclude that separate encoders must normally be present. It sometimes happens that two separately encapsulated tendon organs are innervated by branches of the same Ib afferent (though too rarely to account for the results of Gregory *et al.* 1985), a circumstance that has been exploited by Fukami (1980) to show that the common output is dominated by only one of the receptors, but that its discharge can be reset by antidromic invasion of an impulse of appropriate phase elicited by suprathreshold stimulation of the normally suppressed receptor. This is the most direct evidence that separate encoders can exist in branching systems of muscle receptors, and it is worth noting therefore that the minimum axonal distance between such a pair of tendon organs reported by Fukami (1980) was 1·1 mm which is virtually identical to the equivalent distance between the dynamic (bag_1) and static (bag_2 or chain) inputs of the larger Ia afferents reconstructed by Banks *et al.* (1982).

The mechanism of summation

If occlusion implies the presence of more than one encoding site somewhere within the preterminal and terminal branches of the Ia sensory ending, how then does summation arise, and how is it possible that the degree of summation is not a constant property of individual spindles but variable within individual response cycles (Figs 3*B*, 4*B* and 5)?

In general, a measure of summation could certainly arise from electrotonic coupling of the encoding sites via the preterminal tree. In fact, this must be presumed to be present at least to some degree (see below). For electrotonic coupling to produce the observed summation, the receptor currents generated by each of the sensory terminals must be

relatively unaffected by the spiking activity of the associated encoding site, whether induced by that receptor potential or by antidromic invasion from a more active encoder elsewhere in the afferent tree. The more active encoding site could only be made more excitable by the addition to its generator current of diminished versions of distant receptor currents. The relative dimensions of the sensory terminals on the one hand, and of the unmyelinated preterminal branches supplying them and the ultimate nodes of Ranvier (the heminodes, which are the likely encoding sites; Quick *et al.* 1980) on the other hand, suggest the presence of an impedance mismatch between the receptor and encoding sites that would indeed permit the above interaction by spread of receptor current. This was readily confirmed in principle by the computer simulations described in the Results, with the reservation, though, that it was relatively easy to generate a measure of summation, provided the space constant was suitably adjusted.

The variation of the degree of summation (C_i) within a given response cycle cannot be accounted for by simple electrotonic coupling. In this condition the momentarily dominant encoding site (generating R_c in eqn (2)) should then be driven by its own receptor current (i_h) and a constant fraction ($k_{ec} i_l$) of a remote receptor current (i_l), where k_{ec} is an electrotonic attenuation constant. If, for simplicity, we assume linear rate–current relations for two separate encoding sites (with constants k_1 and k_2) and substitute $R_c = k_1(i_h + k_{ec} i_l)$, $R_h = k_1 i_h$ and $R_l = k_2 i_l$, C_i emerges as a constant: $C_i = k_{ec} k_1 / k_2$. However, as pointed out above (see Methods; Measurement of pacemaker interaction), probabilistic mixing of impulse trains (with finite interval variability) from separate peripheral encoding sites at a common central output node can cause increases in mean discharge rate, even if collision, antidromic invasion and encoder resetting take place, provided the difference between the separate peripheral discharge rates is small. In contrast, if peripheral site discharge rates differ significantly, central site discharge rate will be identical to that of the momentarily dominant peripheral site. This was first proposed by Eagles & Purple (1974) who computed interaction patterns of probability density distributions, and it was then confirmed both experimentally (Hulliger & Noth, 1979) and in computer simulations of impulse generation in preterminal sensory branch trees (Otten, Hulliger & Schaafsma, 1991; Otten *et al.* 1995*b*; and unpublished observations). If probabilistic mixing of separate peripheral site discharge patterns is combined with a measure of summation due to electrotonic spread of receptor currents, the peaked dependence of the degree of summation (C_i) on peripheral site discharge rate difference (Fig. 6) would be expected. In addition, as described under Results (model simulations) critically tuned adaptation properties could further augment cycle phase-dependent variations of the degree of summation. The above computer simulations suggested that under special experimental conditions this could take place on a sufficiently large scale to mask partial summation, generating apparent hyperocclusion.

The effects of tree topology on pacemaker competition

The range of topological structure exhibited by the Ia preterminal-branch trees in the present sample was broadly similar to that of an equivalent sample studied previously by Banks (1986). The similarity extended to such details as the numbers of nodes in the trees, the proportions that were branched (dichotomously or otherwise), and the proportions and orders of ultimate branches that supplied the different types of intrafusal fibre. The main difference of immediate relevance was that in the sample ($n = 16$) of Banks (1986) the first-order branches always supplied the bag_1 and bag_2/chain systems separately, thus emphasizing the unusual nature of afferents Ia.1 and Ia.9 in the present study.

The main question addressed here was whether the degree of occlusion, taken as an indicator of the extent to which pacemaker competition dominated Ia discharge, could be in any way related to the topology of the preterminal-branch structure of the receptor. The prediction was that larger separation of putative encoding sites should manifest itself by higher degrees of occlusion, and this was borne out both by the correlated histophysiological results and by the computer simulations. If electrotonic coupling is at least partly responsible for summation, we should expect that the degree of summation (as measured, for instance, by C_i) would be a negative exponential function of the electrotonic distance between the coupled encoding sites. There is some evidence from our results that this is so. Figure 12*A* illustrates that for the main protocols of this study C_i indeed decreased broadly exponentially as path length increased. The exponential relationship cannot, however, be pressed too far since it is essentially dependent on the fact that the only ending to show high dynamic–static summation was the ending of afferent Ia.1 with the extremely low MPL value of 1, an association which we nevertheless regard as particulary significant in view of the highly unusual nature of its topology. However, other factors are also likely to be involved, in addition to those discussed above: an example, the number of endings supplied by an individual Ia axon, is illustrated in Fig. 12*B*, which shows a weak tendency for C_i to increase with the number of terminals supplied by an individual Ia axon. Other things being equal (MPL, number of internodes), perhaps larger numbers of terminals might generate larger compound receptor currents in remote terminals and, for certain constellations of fusimotor activation of these terminals, larger electrotonic spread from remote sites to a momentarily dominant encoding site.

The proposed mechanism of summation, by its generality, should allow us to predict the output of a spindle primary ending during combined dynamic and static stimulation, knowing the separate outputs in response to dynamic and static stimulations alone and the structure of the Ia preterminal tree. For simplicity we assume that the discharge rates under separate stimulation are unaffected by the tree structure, that different proportions of them, $k_h R_h$ and $k_l R_l$, contribute to the combined discharge rate, R_c, and

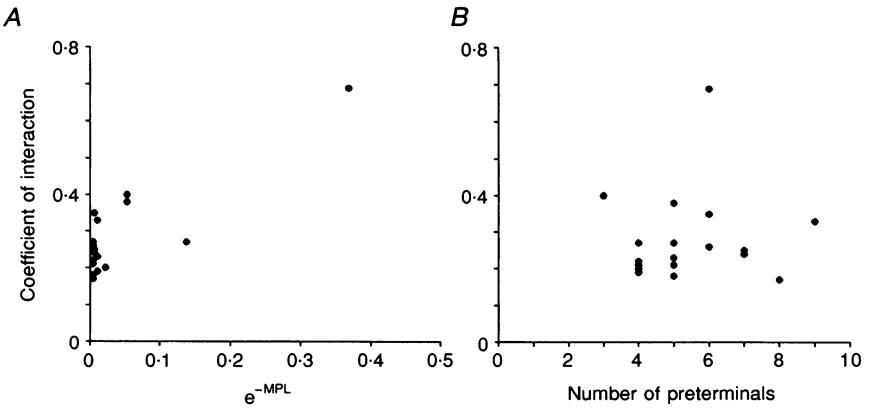

Figure 12. Dependence of pacemaker interaction on preterminal-tree structure

The dependence of average values of C_i on aspects of pre-terminal tree structure. For each point, C_i is the average of values calculated from 200 ms bins where the separate static- and dynamic-activated responses differed by < 10 impulses s^{-1}. *A*, C_i *vs.* e^{-MPL}; *B*, C_i *vs.* the number of ultimate preterminal myelinated branches (referred to, in short, as 'preterminals'). Data are derived from the responses to trapezoidal stretch (protocol T1, see Methods).

that the receptor potential associated with the encoder having the momentarily lower intrinsic discharge rate, R_l, contributes an additional tree-dependent component that can be expressed in terms of R_l as $k_t e^{-MPL} R_l$. Thus, the combined discharge rate,

$$R_c = k_h R_h + k_l R_l + k_t e^{-MPL} R_l. \quad (3)$$

Despite the simplifications in its formulation, this relationship proved to be a quite accurate descriptor of combined discharge rate (Fig. 13). The values of k_h, k_l and k_t were estimated from experimentally observed discharge rates (same data as in Fig. 6) using multivariate regression analysis (see Methods). The particular relationship of eqn (3) was the one that gave the best fit among numerous possibilities which were examined. Again, this must not be overrated, since it cannot be guaranteed that the fit of the data of Fig. 13 represented an overall and not just a local optimum in multivariate space. On the other hand, this general reservation should not detract from the observation that eqn (3) appears to describe the experimental findings remarkably well, if it is borne in mind that other contributing factors, like probabilistic mixing of input trains and discharge rate-dependent adaptation, are not accounted for in this expression. Factors like these may therefore be quite likely sources of the still appreciable variability in the scatter plot of Fig. 13.

Functional implications: why pacemaker competition?

The main finding of functional relevance was that interaction between static and dynamic inputs to spindle Ia afferents was dominated by occlusion, and that remarkably short path lengths between putative encoding sites were

Figure 13. Comparison of predicted with measured Ia discharge during combined static and dynamic activation

Scatter plot of the relationship between (i) the measured Ia afferent discharge rates during combined static and dynamic fusimotor stimulation, both with trapezoidal stretch and at constant muscle length, and (ii) the predicted rates calculated using the empirically derived formula:

$$R_c = k_h R_h + k_l R_l + k_t e^{-MPL} R_l,$$

where R_c is the discharge rate during combined fusimotor stimulation, R_h is the momentarily higher and R_l the momentarily lower discharge rates during separate fusimotor stimulation, k_h, k_l and k_t are empirically derived constants, and MPL is the minimum path length connecting the putative encoding sites (see Discussion). Individual points are calculated on the basis of data averaged in 200 ms bins. There is evidently a close agreement between the predicted and measured discharge rates.

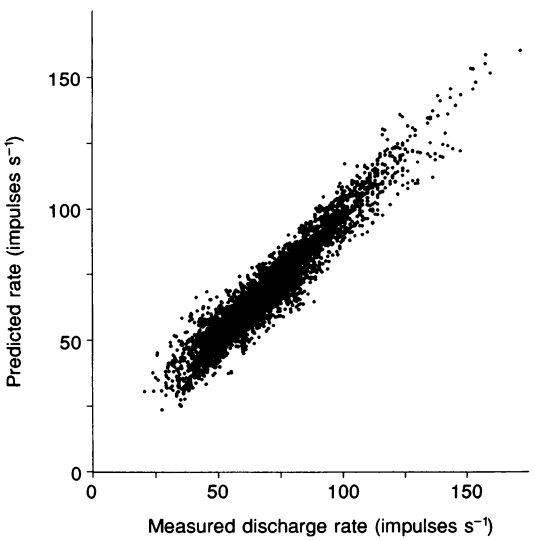

required to allow significant summative interactions to develop. Great variability in the details of Ia preterminal branching is a feature of the spindle primary ending, yet the (usually 2) first-order branches, which might lie immediately alongside each other for several hundred micrometres, quite constantly supply the bag_1 and bag_2-chain system separately (Banks *et al.* 1982; Banks, 1986). The first-order division to the bag_1 and bag_2-chain systems could thus be seen as an adaptation to ensure a highly competitive interaction between encoding sites influenced separately by static and dynamic fusimotor inputs. Thus, rather than operating as an averaging device, the spindle may be viewed as a sensor with certain multiplexer characteristics, since it appears to preserve in unattenuated form, on the basis of momentary switching between separate pacemakers, dominant features of the distinctive information produced by static and dynamic fusimotor action, even when both fusimotor systems are active concomitantly. However, the use that the CNS makes of such a multiplexed signal in motor control and whether more pronounced summation would compromise that control require further functional and modelling studies.

Banks, R. W. (1986). Observations on the primary sensory ending of tenuissimus muscle spindles in the cat. *Cell and Tissue Research* **246**, 309–319.

Banks, R. W. (1991). The distribution of static γ-axons in the tenuissimus muscle of the cat. *Journal of Physiology* **442**, 489–512.

Banks, R. W. (1994*a*). The motor innervation of mammalian muscle spindles. *Progress in Neurobiology* **43**, 323–362.

Banks, R. W. (1994*b*). Intrafusal motor innervation: a quantitative histological analysis of tenuissimus muscle spindles in the cat. *Journal of Anatomy* **185**, 151–172.

Banks, R. W., Barker, D. & Stacey, M. J. (1982). Form and distribution of sensory terminals in cat hindlimb muscle spindles. *Philosophical Transactions of the Royal Society of London* B **299**, 329–364.

Banks, R. W., Hulliger, M., Otten, E. & Scheepstra, K. A. (1993). The Ia afferent of the muscle spindle as an example in the study of pacemaker interactions in branched myelinated axons, both model and real. *Proceedings of the International Union of Physiological Sciences* vol. XVIII, P322.3.

Banks, R. W., Hulliger, M., Scheepstra, K. A. & Otten, E. (1995). Pacemaker competition and the role of preterminal-branch tree architecture: a combined morphological, physiological and modelling study. In *Alpha and Gamma Motor Systems*, ed. Taylor, A., Gladden, M. H. & Durbaba, R., pp. 255–260. Plenum Press, New York.

Baumann, T. K., Emonet-Dénand, F. & Hulliger, M. (1983). Temporal characteristics of the sensitivity-enhancing after-effects of fusimotor activity on spindle Ia afferents. *Brain Research* **258**, 139–143.

Baumann, T. K. & Hulliger, M. (1991). The dependence of the response of cat spindle Ia afferents to sinusoidal stretch on the velocity of concomitant movement. *Journal of Physiology* **439**, 325–350.

Carr, R. W., Morgan, D. L. & Proske, U. (1996). Impulse initiation in the mammalian muscle spindle during combined fusimotor stimulation and succinyl choline infusion. *Journal of Neurophysiology* **75**, 1703–1713.

Celichowski, J., Emonet-Dénand, F., Laporte, Y. & Petit, J. (1994). Distribution of static γ-axons in cat peroneus tertius spindles determined by exclusively physiological criteria. *Journal of Neurophysiology* **71**, 722–732.

Crowe, A. & Matthews, P. B. C. (1964). Further studies of static and dynamic fusimotor fibres. *Journal of Physiology* **174**, 132–151.

Eagles, J. P. & Purple, R. L. (1974). Afferent fibers with multiple encoding sites. *Brain Research* **77**, 187–193.

Emonet-Dénand, F., Hulliger, M., Matthews, P. B. C. & Petit, J. (1977*a*). Factors affecting modulation in post-stimulus histograms on static fusimotor stimulation. *Brain Research* **134**, 180–184.

Emonet-Dénand, F., Hunt, C. C. & Laporte, Y. (1985). Effects of stretch on dynamic fusimotor after-effects in cat muscle spindles. *Journal of Physiology* **360**, 201–213.

Emonet-Dénand, F., Laporte, Y., Matthews, P. B. C. & Petit, J. (1977*b*). On the subdivision of static and dynamic fusimotor actions on the primary ending of the cat muscle spindle. *Journal of Physiology* **268**, 827–861.

Frei, J. B., Hulliger, M. & Lengacher, D. (1981). A programmable wide-range analogue signal generator based on digital memories for use in physiological experiments. *Journal of Physiology* **318**, 2–3*P*.

Fukami, Y. (1980). Interaction of impulse activities originating from individual Golgi tendon organs innervated by branches of a single axon. *Journal of Physiology* **298**, 483–499.

Fukami, Y. (1981). Responses of isolated Golgi tendon organs of the cat to muscle contraction and electrical stimulation. *Journal of Physiology* **318**, 429–443.

Gioux, M., Petit, J. & Proske, U. (1991). Responses of cat muscle spindles which lack a dynamic fusimotor supply. *Journal of Physiology* **432**, 557–571.

Gregory, J. E., Morgan, D. L. & Proske, U. (1985). Site of impulse initiation in tendon organs of cat soleus muscle. *Journal of Neurophysiology* **54**, 1383–1395.

Hulliger, M. (1984). The mammalian muscle spindle and its central control. *Reviews in Physiology, Biochemistry and Pharmacology* **101**, 1–110.

Hulliger, M. & Baumann, T. K. (1994). Component analysis of the responses of sensory neurons to combined sinusoidal and triangular stimulation. *Journal of Neuroscience Methods* **53**, 173–188.

Hulliger, M., Matthews, P. B. C. & Noth, J. (1977). Effects of combining static and dynamic fusimotor stimulation on the response of the muscle spindle primary ending to sinusoidal stretching. *Journal of Physiology* **267**, 839–856.

Hulliger, M. & Noth, J. (1979). Static and dynamic fusimotor interaction and the possibility of multiple pace-makers operating in the cat muscle spindle. *Brain Research* **173**, 21–28.

Hunt, C. C. (1990). Mammalian muscle spindle: peripheral mechanisms. *Physiological Reviews* **70**, 643–663.

Kröller, J., Grüsser, O.-J. & Weiss, L. R. (1990). A study of the encoder properties of the muscle-spindle primary afferent fibers by a random noise disturbance of the steady stretch response. *Biological Cybernetics* **63**, 91–97.

Lennerstrand, G. (1968). Position and velocity sensitivity of muscle spindles in the cat. IV. Interaction between two fusimotor fibres converging on the same spindle ending. *Acta Physiologica Scandinavica* **74**, 257–273.

MATTHEWS, P. B. C. & STEIN, R. B. (1969). The sensitivity of muscle spindle afferents to small sinusoidal changes of length. *Journal of Physiology* **200**, 723–743.

NELDER, J. A. & MEAD, R. (1965). A simplex method for function minimization. *Computer Journal* **7**, 308–313.

OTTEN, E., HULLIGER, M. & SCHAAFSMA, A. (1991). Spike transmission in bifurcating terminal axon trees: competition of signals from γ_S- and γ_D-activated spindle compartments. A theory. In *Proceedings of the Symposium on Muscle Afferents and Spinal Control of Movement*, p. 30. Société des Neurosciences, Paris.

OTTEN, E., HULLIGER, M. & SCHEEPSTRA, K. A. (1995*a*). A model study on the influence of a slowly activating potassium conductance on repetitive firing patterns of muscle spindle primary endings. *Journal of Theoretical Biology* **173**, 67–78.

OTTEN, E., SCHEEPSTRA, K. A. & HULLIGER, M. (1995*b*). An integrated model of the mammalian muscle spindle. In *Alpha and Gamma Motor Systems*, ed. TAYLOR, A., GLADDEN, M. H. & DURBABA, R., pp. 294–301. Plenum Press, New York.

PRICE, R. F. & DUTIA, M. B. (1989). Physiological properties of tandem muscle spindles in neck and hind-limb muscles. *Progress in Brain Research* **80**, 47–56.

QUICK, D. C., KENNEDY, W. R. & DONALDSON, L. (1979). Dimensions of myelinated nerve fibers near the motor and sensory terminals in cat tenuissimus muscles. *Neuroscience* **4**, 1089–1096.

QUICK, D. C., KENNEDY, W. R. & POPPELE, R. E. (1980). Anatomical evidence for multiple sources of action potentials in the afferent fibers of muscle spindles. *Neuroscience* **5**, 109–115.

SCHAAFSMA, A., OTTEN, E. & VAN WILLIGEN, J. D. (1991). A muscle spindle model for primary afferent firing based on a simulation of intrafusal mechanical events. *Journal of Neurophysiology* **65**, 1297–1312.

SCHEEPSTRA, K. A., OTTEN, E., HULLIGER, M. & BANKS, R. W. (1995). Modelling of chaotic and regular Ia discharge during fusimotor stimulation. In *Alpha and Gamma Motor Systems*, ed. TAYLOR, A., GLADDEN, M. H. & DURBABA, R., pp. 325–327. Plenum Press, New York.

Acknowledgements

This study was supported by research grants from the Canadian MRC (to M.H.) and from The Wellcome Trust (to R.W.B.); and by a studentship from the Netherlands Science Foundation (to K.A.S.). We also wish to acknowledge the engineering assistance provided by W. M. Morrow (software design) and B. Kacmar (electronics), and assistance with histology by Christine Richardson. We are very grateful to Dr R. Hawkes for making available to us the facilities of the electron microscopy unit of the University of Calgary Medical School.

Author's email address

R. W. Banks: r.w.banks@durham.ac.uk

Received 29 August 1996; accepted 19 September 1996.